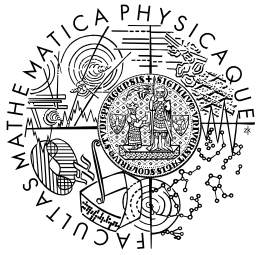

FACULTY
OF MATHEMATICS
AND PHYSICS
Charles University

HABILITATION THESIS

RNDr. Jan Kunc, Ph.D.

Epitaxial Graphene on Silicon Carbide

Institute of Physics of Charles University

Prague 2021

The page left intentionally blank.

Contents

Introduction

Graphene, as a two-dimensional allotrope of carbon, triggered great attention in 2004. I will describe a brief history of graphene, its basic electronic and optical properties, growth methods, and my contribution to the topic. I entered the field relatively late, in 2011, when I came as a postdoc in the group of professor Walter A. de Heer at the Georgia Institute of Technology. However, the field was not entirely new to me because I did my Ph.D. in Dr. Marek Potemski's group in the Grenoble High Magnetic Field Laboratory, where part of his team was intensively involved in the problematics since the early days of graphene. Discussions and group meetings with my supervisor Marek Potemski, colleagues Milan Orlita, Clement Faugeras, Duncan Maude, or Paulina Plochocka helped me have a good overview of what is happening in the field of this wonder material at the time of its rise. The discussions of the existence or non-existence of the bandgap were coming and going on an everyday basis. At that time, I was an unbiased observer. I only watched the competition between groups involved in graphene grown by various methods. I will make my best effort here to express my opinion that all graphene types were probably equally important at the beginning. They mutually excited the field, and they all together led to the success story of graphene. However, I shall admit I got a bit biased during my postdoctoral stay in Atlanta, where I got hands on the epitaxial graphene.

1. A Brief History of Graphene

The graphene's vibrant history will be the focus of the following introduction. Today's world-wide known material graphene gained its vast attention in 2004. The story started with papers of the three research groups, Novoselov and Geim [16] in Manchester, Walter A. de Heer [17] in Atlanta, and Philip Kim [18] in New York. It was not easy to obtain graphene samples at that time, and per weight, graphene was considered one of the most expensive materials. The fabrication difficulties were probably why many researchers used the so called mechanically exfoliated graphene in the early days of graphene. The easy method of the scotch tape was undoubtedly attractive to get a sample of the unique material. Imagine, this was a time when the only high-quality two-dimensional electron or hole gas materials were primarily molecular beam epitaxy (MBE) grown GaAs, CdTe, and other semiconductor quantum wells. The synonym for MBE, being the mostly broken equipment, is self-explanatory, that the process of growing such heterostructures was far from simple. Suddenly, a scotch tape and graphite appeared, not only allowing fabrication of the high-quality electron or hole gases, but this material also allowed to get to the pure two-dimensional limit (one atom thick layer) and study the linear electronic dispersion apart from the well-known parabolic energy spectrum.

So, how did the graphene boom begin? Geim and Novoselov were relatively new to the field of carbon materials, and this field was instead their field of interest in a free time [19]. Despite that, they came with the breakthrough idea of isolating single graphene sheets in Manchester, United Kingdom.

The graphene's story formed parallel on the other side of the Atlantic. The group of prof. Walt A. de Heer had been already working on carbon nanotubes (CNT) at the Georgia Institute of Technology for a decade, since 1995. The electronic structure of CNT was well-known, but CNT electronics was far from commercialization due to difficulties in an organized ordering of CNTs and growth of a given type of CNT. The idea came up to unwrap the CNT, where the eigenstates are not too different from their closed versions, as Wakabayshi showed [20]. The difference is in the boundary conditions. Solid hard-wall (say, for simplicity), and the periodic boundary conditions. Prof. Walt A. de Heer came with the idea of graphene-based electronics in the early 2000s and filed the US patent on June 12, 2003 (Patent number: 7015142) Provisional application No. 60/477,997. The patent was granted on March 21, 2006. In the meanwhile, other groups worked on a similar problem. Can we use a field effect in metals? This task is somewhat tricky since metals have minimal screening length, and the device would have to be on a sub-nanometer scale. Instead, semimetals provide the small density of states in the vicinity of the Fermi level. One of the typical representatives of semimetals is graphite. Indeed, the field-effect was demonstrated in the work of Novoselov and Geim in 2004 [16].

The third group involved in the early days of the graphene boom was Philip Kim's group at Columbia University. They measured an unusual quantum Hall effect and non-trivial Berry's phase in graphene [18]. They reported the unusual quantum Hall effect in Nature's same issue together with a similar investigation of Geim and Novoselov [21]. The group of P. Kim also confirmed the field effect

in graphene [22].

The ongoing research accelerated enormously. The similarity of the energy dispersion to two-dimensional Dirac fermions allowed verification of the long-predicted Klein tunneling. The possibility of such testing was suggested by Katsnelson, Geim, and Novoselov [23] and indirectly verified by Young and Kim [24]. Sadowski, Potemski and de Heer's group showed the $\sqrt{B}$-Landau level scaling by magneto-optical spectroscopy of ultrathin graphite layers [0]. Other two-dimensional crystals were demonstrated soon by Novoselov and Geim [25]. This discovery triggered another enormous interest in these ultrathin crystals. Nair's experiments demonstrated that solely the fine structure constant defines the optical transparency of graphene in the visible spectral range [26] and no material properties are involved.

Hence, the field-effect in a semimetal, unusual quantum Hall effect, optical transparency in terms of fundamental constants, an analogy with Dirac fermions, and discovery of other purely two-dimensional crystals led to a Nobel prize in physics in 2010 for Novoselov and Geim. Despite the undoubtful contribution to physics, opening entirely new fields of two-dimensional crystals, some researchers criticized their work. The first paper of Novoselov 2004 says that "planar graphene itself has been presumed not to exist in the free state, being unstable with respect to the formation of curved structures such as soot, fullerenes, and nanotubes" [16]. The authors repeated the same in their Nature paper a year later "This material has not been studied experimentally before and, until recently, was presumed not to exist in the free state" [21]. Although these inaccuracies would probably be unseen or forgotten if the authors of these papers did not receive the Nobel prize, it is educative to know that all scientists make mistakes from time to time. Indeed, there was relatively intense research of the graphite monolayers starting in the 1980s. There are already review papers on this topic [28, 27] by the end of the 1990s. The term "graphene" was defined by H.P.Boehm in 1985 [29], and the nomenclature was officially adopted at the International Union of Pure and Applied Chemistry (IUPAC) in 1994. In spite of that, the term monolayer graphite was still commonly used. Surprisingly enough, the first measurement of the Dirac linear dispersion by Angular Resolved Photoelectron Spectroscopy (ARPES) was reviewed in Oshima [28], and some signatures of decoupled graphene overlayers on graphite might be recognized already in Takahashi in 1985 [30]. However, the reader should be aware that these early studies dealt with graphene on metal surfaces or transition metal carbides. No attention was paid to grow graphene on an insulating substrate for transport measurements. Ruoff's group made some attempts in this direction to exfoliate a Highly Oriented/Ordered Pyrolytic Graphite (HOPG) by Atomic Force Microscopy (AFM) mechanically. However, not very successfuly [31]. The incorrect statement that graphene, the monolayer of graphite, has not been studied experimentally before and thought not to exist in the free state was corrected by a more in-depth literature search in Geim's paper in 2012 [19]. The work of B. Brodie 1859 [32] was acknowledged as probably the first experimental realization of graphene, although the graphene's presence was not proved, not even searched. Based on our current knowledge, we can only guess that the graphite exposure to strong acids truly produced, besides others, also graphene. Similarly, we can look at the history of epitaxial graphene on SiC. The first experimental realization of the same

can be traced back to Acheson's patent (No. 492,767), E.G. Acheson, Production of Artificial Crystalline Carbonaceous Materials, Carborundum Company, Pennsylvania, USA, 1893. However, these discoveries, in my opinion, cannot be considered as the first works related to graphene. It would be similar to say that plasmonics started in Middle Ages because the colored windows in cathedrals are due to the plasmon absorption on metal nanoparticles or that graphene started with coal discovery.

The first intentional studies of monolayer graphene could be possibly the work of van Bommel [33], who examined monolayer graphene on SiC by Low Energy Electron Diffraction (LEED) and Auger spectroscopy. However, he did not show the monolayer nature of the studied material. Other such disputable observations are Dirac spectrum by ARPES in the work of Takahashi [30]. On the other hand, the graphene on metal surfaces and transition metal carbides, reviewed by Oshima in 1997 [28] already brought strong evidence of graphene as a monolayer of graphite, including signatures of linear bandstructure in the vicinity of the K and K' points. The ongoing work of Forbeaux also showed how graphene could be grown on SiC [34].

However, it was not until 2004, when the high-quality graphene with mobility on the order of 10 000 $cm^2V^{-1}s^{-1}$ was demonstrated [16] together with clear evidence of the linear dispersion of Dirac fermions and unusual quantum Hall effect [21, 18].

A long story short, it should be clear now that all statements that graphene was invented in 2004 are incorrect. The true story is that the interest in graphite monolayers was marginal before 2004, and the high quality of mechanically exfoliated graphene and easiness of producing large-scale graphene on the electronic grade SiC were at the beginning of the graphene boom. I somehow doubt that epitaxial graphene by itself would drive such broad interest in the scientific community since the carrier mobilities at room temperature were about 1000 $cm^2V^{-1}s^{-1}$. The mechanically exfoliated graphene would probably never drive such attention for its low yield of fabrication methods. Both together showed great potential as a new material besides the widespread silicon or even high-quality electron/hole gases in GaAs and CdTe.

As can be seen in Fig. 1.1 the rise of graphene was huge. The first competitors, exfoliated and epitaxial graphene, were soon accompanied by graphene prepared by chemical vapor deposition (CVD). Chemists took their chance by promoting the idea of large scale production; the reduced graphene oxide reappeared on the scene after almost 150 years [32]. The CVD growth of graphene was, of course, also well-known by that time. However, the first attempts gained relatively poor quality graphene, and the mainstream research did not pay too much attention to CVD graphene. The research of exfoliated graphene mostly evolved in the study of the high-quality electron gas. The exfoliated graphene embedded in BN exhibited further improved carrier mobility. The CVD graphene is these days (2021) on a similar level as epitaxial graphene. However, the most challenging part of the fabrication process remains the transfer from the metal catalyst to the insulating substrate.

Until today, the Web of Science collects about 240 000 papers published on a topic "graphene". This enormous amount of papers is clearly off of the abilities of any human being to read them all or to have any overview of what is happen-

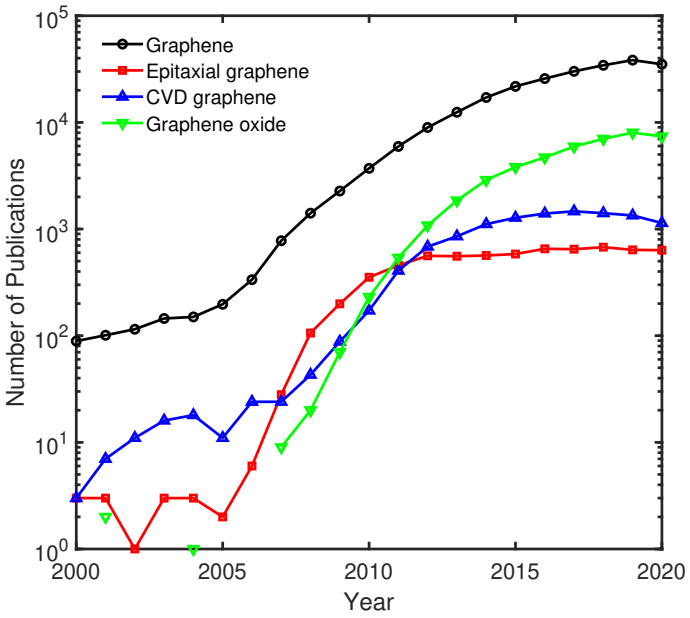

Figure 1.1: Number of publications per year according to Web of Science, topic: (black) graphene, (red) epitaxial graphene or SiC graphene, (blue) CVD graphene, (green) graphene oxide.

ing in all particular notches of graphene research. The intense research is also reflected in the number of almost 3000 review papers on different aspects of this research field. One can find broad review articles on the electronic properties of graphene [35], Raman spectroscopy [36], photonics and optoelectronics [37], graphene oxide [38], transistors [39], functionalization of graphene [40], graphene composites [41], thermal properties [42], photodetectors [43], plasmonics [46, 45, 44], structural defects [47], electrochemical sensors and biosensors [48], photonics [45], transparent electrodes [49] or supercapacitors [50], or biological interactions of graphene [51]. I have selected only those reviews which are more than seven hundred times cited.

For this reason, I will primarily focus on the progress of epitaxial graphene on SiC. The first works of W. A. de Heer were soon followed by groups initially working on SiC. The first works focused on band structure measurements of graphitic layers grown on SiC(0001) [52], or the bilayer graphene band structure studied by ARPES in the work of Ohta [53]. Seyller brought up the importance of the graphitic layers for forming ohmic contacts to SiC [52, 54].

Lanzara's group showed that epitaxial graphene on the C face of SiC contains about 20-30% of AB stacked (graphite-like) bilayers and about 20% of trilayers [55]. Although graphene on the carbon face is not so much studied as graphene on the Si face of SiC, Lanzara's finding is essential for correct interpretations of far-infrared spectroscopy or X-ray. Weng [56] observed the AB-stacking in multilayer epitaxial graphene (MEG) by electron diffraction and high-resolution Trasmission Electron Microscopy (TEM). Orlita [57] observed similar structures in graphite. The Landau level spectroscopy shows a bilayer-like Landau fan chart, which indicates AB stacked graphene layers. These conclusions were further verified by Johansson [58] and commented by Sprinkle [59] and Tajeda [60]. Sun [61]

determined the screening length in MEG to be roughly 1-2 atomic layers wide, the results verified by Ohta [0].

Norimatsu and Kusunoki showed that graphene on SiC is terminated directly into the SiC substrate [62, 63]. Such termination is a significant difference from all other graphenes (exfoliated, CVD, reduced graphene oxide, suspended, graphene flakes on graphite) because there are no sites where external molecules can react with graphene. This termination makes epitaxial graphene unique in terms of chemical reactivity. Though graphene is known to be chemically inert; however, its edges are very reactive. The termination of epitaxial graphene makes the edges perfectly passivated, and they provide high chemical robustness unseen in any other graphenes. This passivation is advantageous for harsh environment operation, but it is a disadvantage for gate oxide growth for transistor applications where special surface pretreatment needs to done [64]. Gaskill's group studied details of surface reactivation for oxide layer growth by atomic layer deposition [65], and they demonstrated the successful fabrication of ultrafast graphene rectifiers [66, 67]

There was an intense discussion about the origin of a bandgap in epitaxial graphene. Bostwick showed that electron-electron, electron–plasmon, and electron-phonon coupling has to be considered equally to understand the dynamics of quasiparticles in epitaxial graphene [68] as measured by ARPES. The alternative explanation provided by Zhou [69] was critically commented in Nature Materials [70, 71]. The first group further discusses the many-body interaction in Ref. [72] and the following work [73]. Bostwick further developed the theory of plasmarons [74] and followed by Walter's study on the screened plasmarons [75].

The crucial technological contribution was a work of Emtsev [76]. This work showed the possibility of growing high-quality graphene in argon at atmospheric pressure. The discussion of Emtsev's [76] argon mediated growth and de Heer's [77] high vacuum growth took almost a decade. We finally resolved this question by our group in Prague [1].

Roehr found minuscule differences between Raman spectra of exfoliated and epitaxial graphene [78]. The work also pointed out the possibility of determining the number of graphene layers by Raman spectroscopy. This method appeared to be a complementary method of the number of layer determination to the work function measurements done by Filleter [79], or low energy (0-8 eV) electron reflectivity spectroscopy [80].

Another essential step in the technology of growth was the work of Riedl [81], who showed a possibility of growing so called hydrogen intercalated epitaxial graphene. The intercalation can proceed by many different elements [82] and methods, where annealing in the air was probably the most surprising one [83], as well as annealing in water vapors [84], or intercalation by thermal shock done by Sumi [85]. However, the intercalation by hydrogen seems to be so far the most promising one. The intercalation decouples the so-called buffer layer from the SiC substrate. The buffer layer electronic structure turns into π-bands of graphene without any localized states. The localized states act as charge traps, and they cause additional scattering. Thus eliminating the buffer layer led to the increase of carrier mobility from 1000 $\mathrm{cm^2V^{-1}s^{-1}}$ to 3000-4000 $\mathrm{cm^2V^{-1}s^{-1}}$ at room temperature and almost temperature-independent carrier mobility from 4K to 300K [86]. The latter being a strong indication of reduced interaction of

carriers with SiC substrate.

Liu observed plasmons by high-resolution electron-energy-loss spectroscopy (HREELS) [87], and Koch observed a strong plasmon-phonon coupling [88]. The phonons are those from the SiC substrate. They are the dominant source of scattering in epitaxial graphene [89]. Crassee studied plasmons, and magneto-plasmons [90] and Chen showed by the near field microscopy that topographical edges of SiC act as boundaries of nano-size plasmons [91] defined by the SiC atomically flat terraces. Cai used these plasmons to demonstrate efficient terahertz detectors [92].

Jobst [93] confirmed by the temperature dependence of the conductance relatively strong coupling to the SiC substrate. When gated by tetrafluoro-tetracyanoquinodimethane (F4-TCNQ) close to the Dirac point, the mobility increases substantially, and the graphene quantum Hall effect occurred. Jobst also found that SiC step edges do not influence the carrier density and mobility. Therefore the steps in SiC are not the dominant scattering centers [89]. Comparing lithographically fabricated Hall bars and shadow masked van der Pauw devices, Jobst also concluded that polymethylmethacrylate (PMMA) residua do not contribute to the additional scattering. Jobst ruled out the adsorbed molecules on the graphene surface. However, he identified the phonon scattering as a dominant scattering mechanism, confirmed by Giesbers evidence of strong electron-phonon coupling [94]. At low temperatures, the residual resistivity indicated crystal imperfections or Coulomb scatterers in the buffer layer or the SiC substrate. Jobst also found ultra-high carrier mobility in the vicinity of the Dirac point, 29 000 $\mathrm{cm^2V^{-1}s^{-1}}$ by using F4-TCNQ. Ristein further studied F4-TCNQ doping [95] and identified a high density of localized states near the Dirac point. These localized states tend to pin Fermi energy, and they were associated with the underlying buffer layer. Lin also studied scattering mechanisms of charge carriers in epitaxial graphene [96] and found the role of point defects, too.

Employing the SiC conducting channel instead of graphene was first demonstrated by Krach [97] and later developed further by Hertel [98]. Waldmann solved the ever problematic back gating of epitaxial graphene by ion implantation of SiC [99]. Our group in Prague contributed to the back gating problematics by an alternative approach, where we grew a thin high resistivity, vanadium doped layers of SiC on top of the conducting SiC substrate [2].

Ferromagnetism in hydrogen intercalated graphene was found by the group of Flipse [100]. The origin was explained just recently by the same group [101].

Giant Faraday rotation in a monolayer and multilayer graphene was observed [102]. As a minor result, I would like to point out here very clean measurements of the Fermi level by mid-far infrared absorption. Crassee also studied a multi-component magneto-optical conductivity of graphene [103] which is essential for the description of the far-infrared optical response modeling. The method of deriving the optical conductivity from the optical transmission data was shown by Orlita [104].

The ever-growing interest in spintronics also touched the epitaxial graphene. Maassen showed quite long spin relaxation times [105] of about 2 ns by measuring the Hanle effect.

Last but not least, the epitaxial graphene is currently, in my opinion, the only candidate on a first application, where the actual graphene's properties could

be employed. This application is the resistance standard, first demonstrated by Tzalenchuk [106] and now its developments are approaching the industrial application.

As the field is immense, I recommend the reader some of the recent reviews on epitaxial graphene [108, 107]. Despite that, the progress in epitaxial graphene keeps its pace, as can be seen from Fig. 1.1 where epitaxial graphene shows a steady interest in the scientific community. The recent progress in, e.g., polymer assisted growth [109], or polymer assisted doping [110] is extraordinary, and the epitaxial graphene is still on a similar footing as the best CVD graphene [111]. The competition and progress are thus still opened, and I can say it is an exciting experience to be part of this story.

2. Basic Properties of Graphene

After exhausting, nevertheless not a complete overview of the graphene's history, I would like to show two exemplary calculations of graphene's basic electronic and optical properties. These will be the electronic band structure and optical transmission. Both calculations can be used in the lectures of solid-state physics for their educative simplicity.

2.1 Electronic Properties

The simplest method to derive electronic dispersion relation in graphene is to use the tight-binding method. The two-dimensional graphene crystal is shown in Fig. 2.1. Each unit cell contains two carbon atoms. These are two identical carbon atoms; however, as can be seen from their bonding to the nearest neighbors, they are not equivalent. These two non-equivalent carbons will be labeled A and B, as shown in Fig. 2.1 by red and blue points.

2.1.1 Wave function

The electronic structure determining the transport and optical properties are given by the energy bands formed by $\tilde{p}_z$ orbitals. These $\tilde{p}_z$ orbitals will form the basis for our tight-binding calculations. In this approximation, the wave function $\varphi_1(\mathbf{r})$, describing an electron on the site A, is simply the $\tilde{p}_z$ orbital located on that site, and similarly for the electron on the site B, hence

$$\begin{aligned} \varphi_1(\mathbf{r}) =& \tilde{p}_z(\mathbf{r}-\mathbf{r}_1) \\ \varphi_2(\mathbf{r}) =& \tilde{p}_z(\mathbf{r}-\mathbf{r}_2). \end{aligned} \tag{2.1}$$

The total wave function $\varphi(\mathbf{r})$ of this unit cell will be the linear combination of the basis functions Eq. (2.1),

$$\varphi(\mathbf{r}) = b_1\varphi_1(\mathbf{r}) + b_2\varphi_2(\mathbf{r}), \tag{2.2}$$

where the b_1 and b_2 are unknown linear coefficients to be determined. We have to construct the wave function Ψ of the whole graphene lattice. This total wave function is the sum of the electron wave functions of all unit cells. In order to construct the wave function in any unit cell, we will use the Bloch theorem. The Bloch theorem says, that the wave function in the periodic crystal comprises of the function $u(\mathbf{r})$ periodic with the lattice and the exponential envelope $e^{i\mathbf{k}\cdot\mathbf{r}}$. Hence, since now we know the wave function $\varphi(\mathbf{r})$ in the unit cell $\mathbf{R} = 0$, we can construct the wave function in any other unit cell given by $\mathbf{r} = \mathbf{R} \neq 0$. The lattice vector $\mathbf{R}$ is given by the linear combination of the lattice vectors $\mathbf{a}_1, \mathbf{a}_2$,

$$\begin{aligned} \mathbf{a}_1 =& a_0\sqrt{3}\left(\frac{1}{2}, \frac{\sqrt{3}}{2}\right) \\ \mathbf{a}_2 =& a_0\sqrt{3}\left(-\frac{1}{2}, \frac{\sqrt{3}}{2}\right), \end{aligned} \tag{2.3}$$

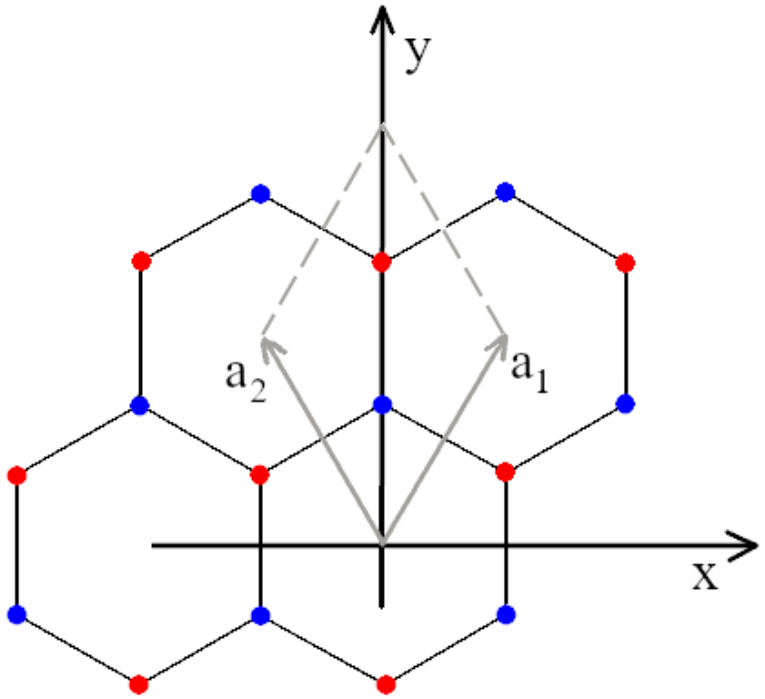

Figure 2.1: Graphene lattice. The red and blue points are the two non-equivalent carbon atoms (A and B site). The graphene lattice vectors a_1 and a_2 are also depicted.

where $a_0 = 1.45$ Å is the carbon-carbon nearest neighbor distance. The position of any unit cell is then $\mathbf{R} = n_1\mathbf{a}_1 + n_2\mathbf{a}_2$, and n_1, $n_2 \in \mathbb{Z}$ are integers. The wave function $\varphi_{\mathbf{R}}(\mathbf{r})$ in the unit cell at the position $\mathbf{R}$ is

$$\varphi_{\mathbf{R}}(\mathbf{r}) = \varphi(\mathbf{r} - \mathbf{R})e^{i\mathbf{k}\cdot\mathbf{R}} \tag{2.4}$$

and the final wave function $\Psi_{\mathbf{k}}(\mathbf{r})$ of the whole graphene lattice is

$$\Psi_{\mathbf{k}}(\mathbf{r}) = \sum_{n_1,n_2} \varphi(\mathbf{r} - \mathbf{R})e^{i\mathbf{k}\cdot\mathbf{R}}. \tag{2.5}$$

2.1.2 Hamiltonian

The hamiltonian H of electrons moving in the graphene lattice consists of the kinetic energy T and potential energy V. The kinetic energy is given by electron mass m_0 in vacuum and momentum $\mathbf{p}$,

$$T = \frac{\mathbf{p}^2}{2m_0}. \tag{2.6}$$

The potential energy around each carbon atom is given by the atomic potential energy $V_{at}(\mathbf{r})$ which localizes the carbon atom on a given site. Hence, the total potential energy of the two carbons in the first unit cell is

$$V(\mathbf{r}, \mathbf{R} = \mathbf{0}) = V_{at}(\mathbf{r} - \mathbf{r_1}) + V_{at}(\mathbf{r} - \mathbf{r_2}). \tag{2.7}$$

The total potential energy $V(\mathbf{r})$ of the whole graphene lattice is a sum over all unit cells

$$V(\mathbf{r}) = \sum_{n_1,n_2} V_{at}(\mathbf{r} - \mathbf{r}_1 - \mathbf{R}) + V_{at}(\mathbf{r} - \mathbf{r_2} - \mathbf{R}). \tag{2.8}$$

2.1.3 Eigenvalue problem

In the following, we have to solve the eigenvalue problem

$$H\Psi_{\mathbf{k}}(\mathbf{r}) = E\Psi_{\mathbf{k}}(\mathbf{r}), \tag{2.9}$$

where the energy $E = E(\mathbf{k})$ depends on the wave vector $\mathbf{k}$. We treat this wave vector dependence as a variable parameter of the eigenvalue problem. We shall solve the eigenvalue problem (2.9) for all wave vectors from the first Brillouin zone. What we do not know are the two linear coefficients b_1 and b_2. Therefore, we need to recast the eigenvalue problem (2.9) into two equations and solve them for two variables b_1 and b_2. We will do so by multiplying (2.9) by $\varphi_1(\mathbf{r})$ and $\varphi_2(\mathbf{r})$ from left and integrating over whole space. These two operations lead to two desired equations, which can be written in the Dirac notation as

$$\langle\varphi_1|H|\Psi_{\mathbf{k}}(\mathbf{r})\rangle = E\langle\varphi_1|\Psi_{\mathbf{k}}(\mathbf{r})\rangle \tag{2.10a}$$

$$\langle\varphi_2|H|\Psi_{\mathbf{k}}(\mathbf{r})\rangle = E\langle\varphi_2|\Psi_{\mathbf{k}}(\mathbf{r})\rangle. \tag{2.10b}$$

We will examine the left hand side of the first equation (2.10a) in detail by inserting the full expression of the wavefunction $\Psi_{\mathbf{k}}(\mathbf{r})$. Hence,

$$\begin{aligned}\langle\varphi_1|H|\Psi_{\mathbf{k}}(\mathbf{r})\rangle = \langle\varphi_1|H|\sum_{n_1,n_2}\varphi(\mathbf{r}-\mathbf{R})e^{i\mathbf{k}\cdot\mathbf{R}}\rangle = \\ \langle\varphi_1|H|\sum_{n_1,n_2}(b_1\varphi_1(\mathbf{r})+b_2\varphi_2(\mathbf{r}))e^{i\mathbf{k}\cdot\mathbf{R}}\rangle,\end{aligned} \tag{2.11}$$

where we have used the linear combination (2.2) of the p_z orbitals on the sublattice A and B. We reorganize the sum over all unit cells (indices n_1 and n_2) and we start with the units cell where is the wave function φ_1 and φ_2 localized. This is the unit cell $n_1 = n_2 = 0$. We rewrite the sum as a sum over the nearest neighbors, next nearest neighbors and so on. Hence,

$$\langle\varphi_1|H|\Psi_{\mathbf{k}}(\mathbf{r})\rangle = b_1\langle\varphi_1|H|\varphi_1\rangle + \sum_{\mathbf{R}\in NN} b_2\langle\varphi_1|H|\varphi_2(\mathbf{r}-\mathbf{R})\rangle e^{i\mathbf{k}\cdot\mathbf{R}} + \sum_{\mathbf{R}\in NNN}\ldots \tag{2.12}$$

We consider only the interaction between the nearest neighbors so we neglect all the terms starting from the third term on the right hand side (RHS) in (2.12). The term $\langle\varphi_1|H|\varphi_1\rangle$ can be evaluated by applying the Hamiltonian H on the wave function φ_1, giving $H\varphi_1 = \epsilon_1\varphi_1$. The ϵ_1 is the energy of the state $|\varphi_1\rangle$. In other words, this is the energy of the carbon atom 1. This energy will be the same for the carbon atom 2, and the same holds for carbons in all other unit cells. Since this is a constant, we can set it $\epsilon_1 = 0$. The remaing part is the sum over the nearest neighbors

$$\langle\varphi_1|H|\Psi_{\mathbf{k}}(\mathbf{r})\rangle \approx \sum_{\mathbf{R}\in NN} b_2\langle\varphi_1|H|\varphi_2(\mathbf{r}-\mathbf{R})\rangle e^{i\mathbf{k}\cdot\mathbf{R}}. \tag{2.13}$$

One can see from Fig. 2.1 that there are three nearest neighbors of the orbital φ_1. The three neighbors are in the unit cells given by the vector $\mathbf{R} = \{\mathbf{0}, -\mathbf{a}_1, -\mathbf{a}_2\}$. We can also notice that the matrix element $\langle\varphi_1|H|\varphi_2(\mathbf{r}-\mathbf{R})\rangle$ is the same for all

three nearest neighbors, so we can adopt a substitution $\gamma_1 = \langle\varphi_1|H|\varphi_2(\mathbf{r}-\mathbf{R})\rangle$. Evaluating the sum, we arrive at

$$\langle\varphi_1|H|\Psi_{\mathbf{k}}(\mathbf{r})\rangle = \gamma_1 b_2 \sum_{\mathbf{R}\in NN} e^{i\mathbf{k}\cdot\mathbf{R}} = \gamma_1 b_2(1+e^{-i\mathbf{k}\cdot\mathbf{a}_1}+e^{-i\mathbf{k}\cdot\mathbf{a}_2}) \stackrel{\text{def.}}{=} \gamma_1 b_2 \alpha(\mathbf{k}), \quad (2.14)$$

where we also defined the function $\alpha(\mathbf{k})$. This step is important, as we will see later, the function $\alpha(\mathbf{k})$ basically determines the graphene dispersion.

We also need to determine the right hand side of Eq. (2.10a). The procedure is similar to what we derived above. We use our energy calibration that the energy of the state $|\varphi_1\rangle$ is $\epsilon_1 = 0$, and we neglect wave function overlap between next and higher order nearest neighbors. Hence, we get from Eq. (2.10a)

$$\langle\varphi_1|\Psi_{\mathbf{k}}(\mathbf{r})\rangle \approx b_1 + \sum_{\mathbf{R}\in NN} \langle\varphi_1(\mathbf{r})|\varphi_2(\mathbf{r}-\mathbf{R})\rangle b_2 e^{i\mathbf{k}\cdot\mathbf{R}}. \quad (2.15)$$

Again, we notice that the nearest neighbor wave function overlap is the same number for all three neighbors, so we define a new constant

$$\gamma_0 \stackrel{\text{def.}}{=} \langle\varphi_1(\mathbf{r})|\varphi_2(\mathbf{r}-\mathbf{R})\rangle \quad (2.16)$$

and the right hand side of Eq. (2.10a) can be simplified by

$$\langle\varphi_1|H|\Psi_{\mathbf{k}}(\mathbf{r})\rangle = \gamma_0 b_1 \alpha(\mathbf{k}). \quad (2.17)$$

The final set of two equations (2.10)

$$\begin{aligned} \gamma_1 b_2 \alpha(\mathbf{k}) &= (b_1 + \gamma_0 b_2 \alpha(\mathbf{k}))E(\mathbf{k}) \\ \gamma_1 b_1 \alpha^*(\mathbf{k}) &= (b_2 + \gamma_0 b_1 \alpha^*(\mathbf{k}))E(\mathbf{k}) \end{aligned} \quad (2.18)$$

can be written in the matrix form

$$\begin{pmatrix} E(\mathbf{k}) & \alpha(\mathbf{k})[\gamma_0 E(\mathbf{k}) - \gamma_1] \\ \alpha^*(\mathbf{k})[\gamma_0 E(\mathbf{k}) - \gamma_1] & E(\mathbf{k}) \end{pmatrix} \cdot \begin{pmatrix} b_1 \\ b_2 \end{pmatrix} = \begin{pmatrix} 0 \\ 0 \end{pmatrix}. \quad (2.19)$$

We are interested in a non-trivial solution, hence the determinant of the matrix in Eq. (2.19) has to be zero. This is already a simple algebra giving the eigenvalues

$$E(\mathbf{k}) = \pm\frac{\gamma_1|\alpha(\mathbf{k})|}{1+\gamma_0|\alpha(\mathbf{k})|} \simeq \pm\gamma_1|\alpha(\mathbf{k})|. \quad (2.20)$$

We also did an approximation in Eq. (2.20) $\gamma_0|\alpha(\mathbf{k})| \ll 1$. This approximation means that the wave function overlap of the two neighboring carbons is negligible. Using our definition of $\alpha(\mathbf{k})$ in Eq. (2.14), the dispersion (2.20) can be written as

$$E(\mathbf{k}) = \pm\gamma_1\sqrt{1+4\cos\left(\frac{ak_x}{2}\right)\cos\left(\frac{\sqrt{3}ak_y}{2}\right)+4\cos^2\left(\frac{ak_x}{2}\right)}. \quad (2.21)$$

The lattice constant a is related to the carbon-carbon nearest distance neighbor by $a = \sqrt{3}a_0$, $a_0 = 1.45$ Å. The dispersion spectrum is depicted in Fig 2.2.

The conduction and valence band touch at the K and K' points in the first Brillouin zone. The coordinate on the k_x axis of the K-point is $\mathbf{K} = \frac{4\pi}{3\sqrt{3}a_0}\mathbf{e}_{\mathbf{k_x}}$.

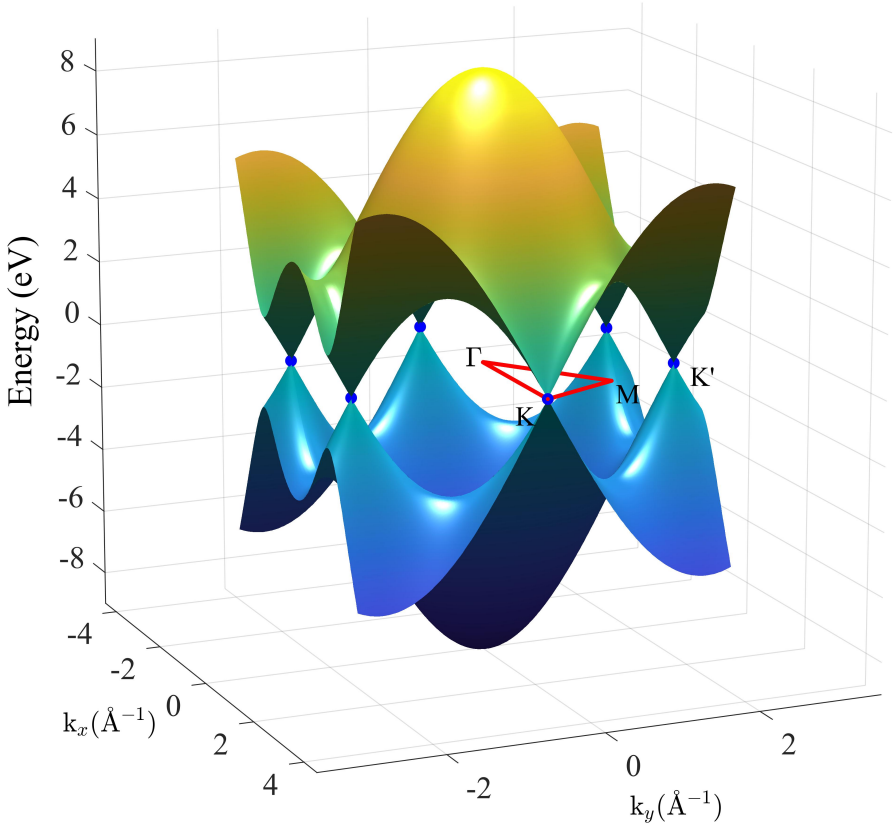

Figure 2.2: Graphene band structure. The blue points show K and K' points. The red line (triangle) is a path between high symmetry points depicted in Fig. 2.3.

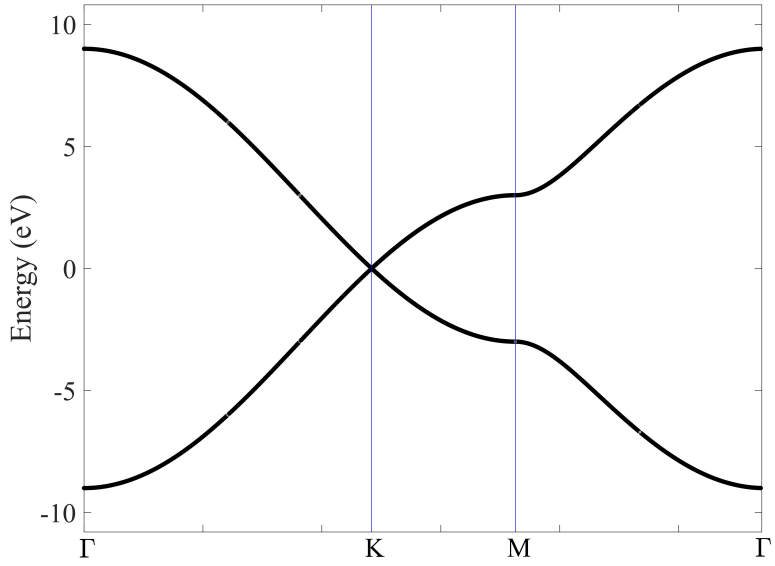

Figure 2.3: Energy band structure of graphene along high symmetry points $\Gamma - K - M - \Gamma$.

2.1.4 Eigenstates

We will calculate the eigenstates by using the simplified dispersion $E(\mathbf{k}) = \pm\gamma_1|\alpha(\mathbf{k})|$. Inserting this dispersion in the first equation in (2.19) and writing $\alpha(\mathbf{k})$ in a general form $\alpha(\mathbf{k}) = |\alpha(\mathbf{k})|e^{i\theta}$ we come to the equation

$$\pm\gamma_1|\alpha(\mathbf{k})|b_1 - |\alpha(\mathbf{k})|e^{i\theta}\gamma_1 b_2 = 0, \tag{2.22}$$

where we have also neglected the nearest neighbor overlap integral $\gamma_0 \to 0$. The relation between the unknown coefficients b_1 and b_2 is than

$$b_2 = \pm b_1 e^{-i\theta}. \tag{2.23}$$

We write the eigenstates in graphene usually as a two-component spinor

$$\mathbf{b} = \frac{1}{\sqrt{2}}\begin{pmatrix} e^{+i\theta/2} \\ \pm e^{-i\theta/2} \end{pmatrix}. \tag{2.24}$$

Meaning of phase θ

We can interpret the phase θ in the eigenstates (2.24) by expanding function $\alpha(\mathbf{k})$ in Taylor series around the K-point. We can write any wave vector $\mathbf{k}$ in the vicinity of the K point as $\mathbf{k} = \mathbf{K} + \mathbf{q}$. This expression defines a wave vector $\mathbf{q}$, which is measured from the K-point. We use our definition of $\alpha(\mathbf{k})$

$$\alpha(\mathbf{k}) = 1 + e^{-i\mathbf{a}_1\cdot\mathbf{k}} + e^{-i\mathbf{a}_2\cdot\mathbf{k}} = 1 + e^{-i\mathbf{a}_1\cdot(\mathbf{K}+\mathbf{q})} + e^{-i\mathbf{a}_2\cdot(\mathbf{K}+\mathbf{q})} \tag{2.25}$$

and the Taylor expansion results in

$$\alpha(\mathbf{q}) = 1 + e^{-i\mathbf{a}_1\cdot\mathbf{K}}(1 - i\mathbf{a}_1\cdot\mathbf{q}) + e^{-i\mathbf{a}_2\cdot\mathbf{K}}(1 - i\mathbf{a}_2\cdot\mathbf{q}). \tag{2.26}$$

Writting $\mathbf{q}$ in polar coordinates $\mathbf{q} = q(\cos\vartheta, \sin\vartheta)$ allows to evaluate the scalar products

$$\begin{aligned} \mathbf{a}_1\cdot\mathbf{q} =& a_0\frac{\sqrt{3}}{2}q(+\cos\vartheta + \sqrt{3}\sin\vartheta) \\ \mathbf{a}_2\cdot\mathbf{q} =& a_0\frac{\sqrt{3}}{2}q(-\cos\vartheta + \sqrt{3}\sin\vartheta \end{aligned}. \tag{2.27}$$

The complex exponentials can be easily evaluated $e^{-i\mathbf{a}_1\cdot\mathbf{K}} = e^{-i\frac{2}{3}\pi}$ and $e^{-i\mathbf{a}_2\cdot\mathbf{K}} = e^{+i\frac{2}{3}\pi}$. The function $\alpha(\mathbf{q})$ then reads

$$\alpha(\mathbf{q}) = 1 + \left(-\frac{1}{2} - i\frac{\sqrt{3}}{2}\right)(1 - i\mathbf{a}_1\cdot\mathbf{q}) + \left(-\frac{1}{2} + i\frac{\sqrt{3}}{2}\right)(1 - i\mathbf{a}_2\cdot\mathbf{q}). \tag{2.28}$$

Using the scalar products (2.27) and simplifying leads to

$$\alpha(q,\vartheta) = -\frac{3}{2}a_0 q e^{-i\vartheta}. \tag{2.29}$$

We recall our general complex form of $\alpha(\mathbf{k}) = |\alpha(\mathbf{k})|e^{i\theta}$, used in Eq. (2.22), the same angle θ later appeared in the eigenfunctions Eq. (2.24). Hence, the relation between these two angles is $\theta = -\vartheta$. The phase factor in the eigenfunctions Eq. (2.24) has a meaning of the polar angle in the vicinity of the K point.

2.1.5 Berry's phase

As we know the eigenstates and we know the interpretation of the phase θ in eigenstates, we can look now at one intriguing property of graphene's wave function. It is the so called non-trivial Berry's phase. The general form of the wavefunction can be written as

$$|\Psi(\mathbf{r},t)\rangle = |n(\mathbf{r},t)\rangle e^{i\Theta(t)}, \tag{2.30}$$

where $|n(\mathbf{r},t)\rangle$ is the stationary solution and $\Theta(t)$ is a phase factor. Our goal will be, assuming we know the function $|n(\mathbf{r},t)\rangle$, what is the phase of the wavefunction $\Theta(t)$. We start with the time Schrödinger equation

$$i\hbar\frac{\partial|\Psi(\mathbf{r},t)\rangle}{\partial t} = H|\Psi(\mathbf{r},t)\rangle. \tag{2.31}$$

Derivation in time gives

$$i\hbar e^{i\Theta(t)}\frac{\partial|n\rangle}{\partial t} - \hbar|n\rangle e^{i\Theta(t)}\frac{\partial\Theta(t)}{\partial t} = H|\Psi(\mathbf{r},t)\rangle. \tag{2.32}$$

We apply a bra vector $\langle\Psi(\mathbf{r},t)|$ from left, giving

$$i\hbar\langle n|\frac{\partial}{\partial t}|n\rangle - \hbar\frac{\partial\Phi(t)}{\partial t} = \langle\Psi|H|\Psi\rangle = E_n. \tag{2.33}$$

The righ hand side is simply energy E_n of the state $|n\rangle$, and we used normalization of the eigenstates $\langle n|n\rangle = 1$. The phase Φ can be solved by integrating Eq. (2.33)

$$\Phi(t) = -\int_0^t \frac{E_n}{\hbar}dt + i\int_0^t\langle n|\frac{\partial}{\partial t}|n\rangle dt. \tag{2.34}$$

The first term in Eq. (2.34) is the so called de Broglie's phase, or dynamical phase $\Phi_{deBroglie} = -\int_0^t \frac{E_n}{\hbar}dt$. This is the common phase gained in time by every stationary solution. This phase linearly scales with time as long as the stationary solution has constant energy. The second term is the Berry's phase, or geometrical phase Φ_{Berry}. Considering the case of graphene, we assume a modified wave function Eq. (2.35)

$$|n\rangle = \frac{1}{\sqrt{2}}\begin{pmatrix}1\\ \pm e^{-i\theta}\end{pmatrix}. \tag{2.35}$$

Then

$$\Phi = \frac{i}{2}\int_0^t \begin{pmatrix}1 & \pm e^{i\theta}\end{pmatrix}\frac{\partial}{\partial t}\begin{pmatrix}1\\ \pm e^{-i\theta}\end{pmatrix}dt = \frac{1}{2}\int_0^t\frac{\partial\theta}{\partial t}dt = \frac{1}{2}\int_0^{2\pi}d\theta = \pi. \tag{2.36}$$

This is quite surprising, because as we go adiabatically around the K-point, the wave function gains a phase which does not depend on time. It is a solely geometrical property of the eigenfunction. We should note here that taking the wave function in the form of Eq. (2.24) might lead to missleading conclusions on a Berry phase $\Phi = 0$. The reason is that the wave function (2.24) already contains the Berry phase. The Berry phase is retrieved than as a limit case of the countour integral [112]. A detailed discussion can be also found in the review [113].

2.1.6 Dirac Hamiltonian

A Dirac hamiltonian is a common model to describe quasi-particles in graphene, and the analogy with relativistic particles is made thereof. The derivation of Dirac hamiltonian is based on the Taylor expansion of the tight-binding hamiltonian in the vicinity of the K and K'-point. Recalling the full hamiltonian

$$H = \frac{p^2}{2m_0} + \sum_{\mathbf{R}} V_{at}(\mathbf{r} - \mathbf{r}_1 - \mathbf{R}) + V_{at}(\mathbf{r} - \mathbf{r}_2 - \mathbf{R}) \tag{2.37}$$

and using the wave functions $\Psi_1(\mathbf{k}, \mathbf{r})$ and $\Psi_2(\mathbf{k}, \mathbf{r})$ of the carbon atoms at the lattice sites A and B

$$\begin{aligned} \Psi_1(\mathbf{k}, \mathbf{r}) &= \sum_{\mathbf{R}} \phi_1(\mathbf{r} - \mathbf{R}) e^{i\mathbf{k}\cdot\mathbf{R}} \\ \Psi_2(\mathbf{k}, \mathbf{r}) &= \sum_{\mathbf{R}} \phi_2(\mathbf{r} - \mathbf{R}) e^{i\mathbf{k}\cdot\mathbf{R}} \end{aligned} \tag{2.38}$$

as the two basis functions, we can write in the Heisenberg matrix representation

$$H = \begin{pmatrix} \langle\Psi_1|H|\Psi_1\rangle & \langle\Psi_1|H|\Psi_2\rangle \\ \langle\Psi_2|H|\Psi_1\rangle & \langle\Psi_2|H|\Psi_2\rangle \end{pmatrix} = \begin{pmatrix} 0 & \gamma_1\alpha(\mathbf{k}) \\ \gamma_1\alpha^*(\mathbf{k}) & \end{pmatrix}. \tag{2.39}$$

We take the approximation of the function $\alpha(\mathbf{k})$ in the vicinity of the K-point

$$\alpha(q, \vartheta) \simeq -\frac{3}{2} a_0 |q| e^{-i\vartheta}, \tag{2.40}$$

and inserting it in (2.39), we get

$$H = -\frac{3}{2} a_0 \gamma_1 \begin{pmatrix} 0 & q_x - iq_y \\ q_x + iq_y & 0 \end{pmatrix}. \tag{2.41}$$

We used the cartesian coordinates for the $\mathbf{q}$ wave vector. Using the Pauli matrices

$$\sigma_x = \begin{pmatrix} 0 & 1 \\ 1 & 0 \end{pmatrix}, \sigma_y = \begin{pmatrix} 0 & -i \\ i & 0 \end{pmatrix}, \text{ and } \sigma_z = \begin{pmatrix} 1 & 0 \\ 0 & -1 \end{pmatrix}, \tag{2.42}$$

we can rewrite the hamiltonian as

$$H = -\frac{3}{2} a_0 \gamma_1 \left[\begin{pmatrix} 0 & q_x \\ q_x & 0 \end{pmatrix} + \begin{pmatrix} 0 & -iq_y \\ iq_y & 0 \end{pmatrix} \right] = -\frac{3}{2} a_0 \gamma_1 (q_x \sigma_x + q_y \sigma_y). \tag{2.43}$$

The final hamiltonian, using a definiton of the Fermi velocity $v_F = -\frac{3}{2\hbar} a_0 \gamma_1$, reads

$$H = v_F \hbar \mathbf{q} \cdot \sigma. \tag{2.44}$$

The spectrum of hamiltonian (2.44) indeed resembles the Dirac cone, as depicted in Fig. 2.4.

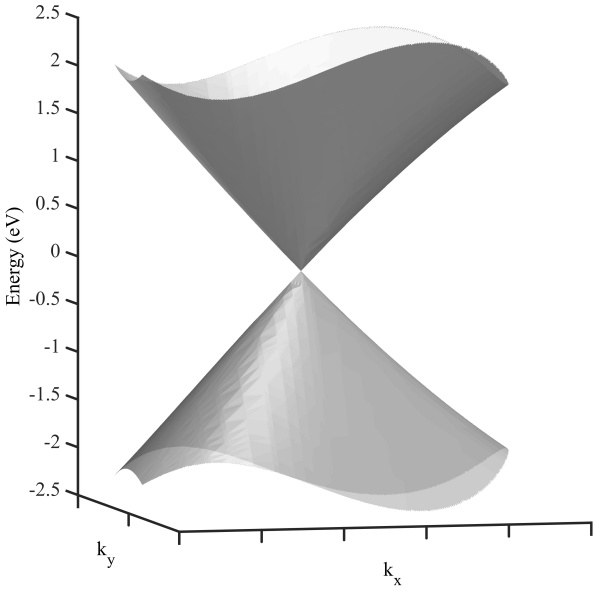

Figure 2.4: Graphene band structure in the vicinity of K and K' points.

2.1.7 Landau Levels

Landau level quantization in the vicinity of the K and K' points is a fingerprint of the graphene monolayer. The Landau level fan chart is calculated by using the Peierls substitution of electron momentum $p \to p + e\mathbf{A}$ in the magnetic field $\mathbf{B}$ described by a vector potential $\mathbf{A}$, $\mathbf{B} = \nabla \times \mathbf{A}$, and elementary charge $e = +1.602 \times 10^{-19}$ C. The Dirac hamiltonian becomes

$$H = v_F(\mathbf{p} + e\mathbf{A}) \cdot \sigma. \tag{2.45}$$

The problem can be solved by searching the eigenvalues of H^2. Say Ψ is the eigenfunction of H, $H\Psi = E\Psi$, then $H^2\Psi = HH\Psi = HE\Psi = E^2\Psi$, and Ψ is also eigenfunctin of H^2. The eigenvalues of H^2 are E^2 and

$$H^2 = v_F^2[(\mathbf{p} + e\mathbf{A}) \cdot \sigma][(\mathbf{p} + e\mathbf{A}) \cdot \sigma]. \tag{2.46}$$

We take the vector potential $\mathbf{A}$ in the Landau gauge

$$\mathbf{A} = \begin{pmatrix} 0 \\ Bx \\ 0 \end{pmatrix}, \tag{2.47}$$

then

$$\begin{aligned} H^2 &= v_F^2[p_x\sigma_x + (p_y + eBx)\sigma_y][p_x\sigma_x + (p_y + eBx)\sigma_y] = \\ &= v_F^2[p_x\sigma_x p_x\sigma_x + (p_y + eBx)\sigma_y p_x\sigma_x + \\ &+ p_x\sigma_x(p_y + eBx)\sigma_y + (p_y + eBx)\sigma_y(p_y + eBx)\sigma_y] \end{aligned} . \tag{2.48}$$

Using the properties of Pauli matrices $\sigma_i^2 = \mathbb{1}$, and their commutation relations $\sigma_x\sigma_y = i\sigma_z$, we arrive at

$$H^2 = v_F^2[p_x^2 + (p_y + eBx)^2 - ieB(xp_x - p_x x)\sigma_z]. \tag{2.49}$$

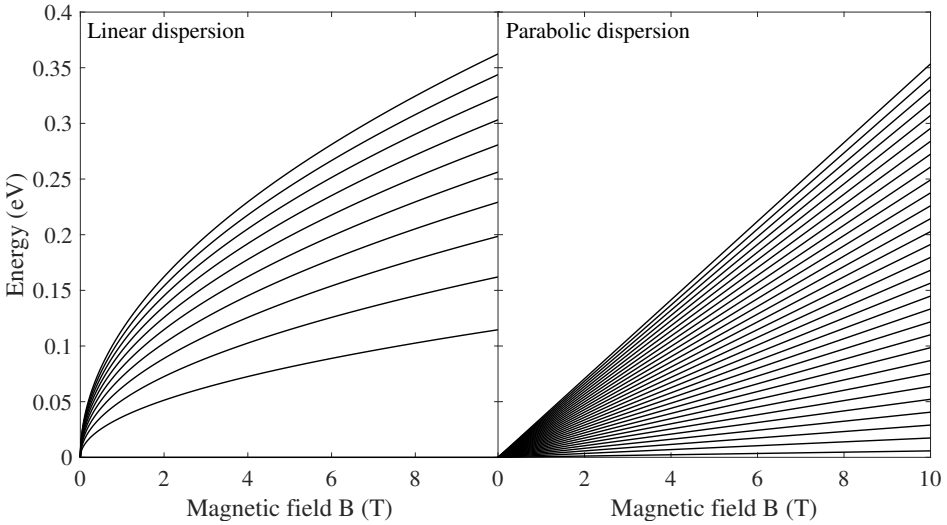

Figure 2.5: Graphene band structure in the vicinity of K and K' points.

The last term contains the commutation relation $[x, p_x] = i\hbar$. We get

$$H^2 = v_F^2[p_x^2 + (p_y + eBx)^2 + eB\hbar\sigma_z]. \tag{2.50}$$

The operator (2.50) resembles the hamiltonian of the free electron in magnetic field. There is additional term $eB\hbar\sigma_z$ which is diagonal in pseudospin eigenstates. We can find the energies in analogy with the spectrum of free electron, taking the substitution $v_F^2 = \frac{1}{2m}$ and knowing $\omega_c = \frac{eB}{m}$ results in

$$E^2 = \hbar\omega_c \left(n + \frac{1}{2}\right) \pm v_F^2 eB\hbar. \tag{2.51}$$

Inserting the substitutions and simple algebra gives

$$E^2 = 2v_F^2 \hbar eB \left(n + \frac{1}{2} \pm \frac{1}{2}\right). \tag{2.52}$$

The quantum number n, $n \in \mathbf{N}$ determines the degeneracy of Landau levels. The quantum number $n = 0$ has two pseudospin split Landau levels at $N = n + \frac{1}{2} \mp \frac{1}{2} = \{0, 1\}$. The quantum number $n = 1$ leads similarly to $N = \{1, 2\}$. The pseudospin splitting is the same as cyclotron resonance. Hence we get pseudospin degenerated spectrum with degeneracy factors $\{1, 2, 2, 2, ...\}$. Including the spin degeneracy leads to degeneracy factors $\{2, 4, 4, 4, ...\}$, and the sequence of integer filling factors is $\{2, 6, 10, 14, ...\}$. The integer filling factors are important in the analysis of the integer quantum Hall effect. The half-filling factor of the first Landau level is related to the Berry phase π. The cyclotron motion of charge carriers rotates the wave function around the K and K' points and probes its phase. The spectrum (2.52) is usually rewritten using the new quantum number N,

$$E = \pm v_F \sqrt{2\hbar eBN}. \tag{2.53}$$

The Landau levels in graphene are compared with a typical semiconductor (CdTe, $m^* = 0.1m_0$) in Fig 2.5.

The $\sqrt{B}$ dependence is a fingerprint of graphene. Another remarkable difference is the large cyclotron gap compared to conventional semiconductors. The consequence is that the quantum Hall effect can be observed at lower magnetic fields and temperatures as high as room temperature [114]. These properties lead currently to the first ongoing application of graphene as a resistance standard.

2.2 Optical Properties

Optical transmission T of monolayer graphene is also remarkable, since it is given only by the fine-structure constant $\alpha \simeq \frac{1}{137}$, $T = 1 - \pi\alpha \simeq 97.7\%$. We will derive the transmission in the semi-classical approximation following the work of Nair [26], where the electromagnetic radiation will be treated classically as vector potential

$$\mathbf{A} = \frac{1}{2}A_0(e^{i\omega t} + e^{-i\omega t}), \tag{2.54}$$

and the Hamiltonian describing the interaction with Dirac fermions is

$$H = v_F\sigma \cdot (\mathbf{p} + e\mathbf{A}). \tag{2.55}$$

We will treat the interaction as a first order perturbation $V = \frac{1}{2}v_F\sigma_x eA_0$. The wavefunctions for the conduction band is

$$\Psi_{CB}(\mathbf{r}) = \frac{1}{\sqrt{2}}\begin{pmatrix} e^{i\theta/2} \\ e^{-i\theta/2} \end{pmatrix} \tag{2.56}$$

and for the valence band

$$\Psi_{VB}(\mathbf{r}) = \frac{1}{\sqrt{2}}\begin{pmatrix} e^{i\theta/2} \\ -e^{-i\theta/2} \end{pmatrix}. \tag{2.57}$$

The matrix element of the optical transition is

$$\langle\Psi_{CB}|V|\Psi_{VB}\rangle = -\frac{i}{2}v_F eA_0 \sin\theta. \tag{2.58}$$

The Fermi's golden rule gives the transition rate $W_{VB\to CB}$ at given wavevector $\mathbf{k}$

$$W_{VB\to CB} = \frac{2\pi}{\hbar}\frac{1}{4}(v_F eA_0 \sin\theta)^2\delta(2\hbar v_F k - \hbar\omega), \tag{2.59}$$

The total transition rate $\frac{1}{\tau}$ is given by contributions $W_{VB\to CB}(k)$ of all wavevectors k, thus integrating (2.59) and taking into account the four-fold degeneracy, we get

$$\frac{1}{\tau} = 4\int \frac{dk_x dk_y}{(2\pi)^2} W_{VB\to CB}(k) = \frac{(e|A_0|)^2\omega}{8\hbar^2}. \tag{2.60}$$

The absorbed energy W_a is

$$W_a = \frac{\hbar\omega}{\tau} = \frac{(e\omega|A_0|)^2}{8\hbar}. \tag{2.61}$$

The vector potential A_0 is related to the electric field E_0 of the electromagnetic wave by $\mathbf{E} = -\frac{\partial\mathbf{A}}{\partial t}$, hence $E_0 = i\omega A_0$. The absorbed energy is

$$W_a = \frac{(eE_0)^2}{8\hbar}. \tag{2.62}$$

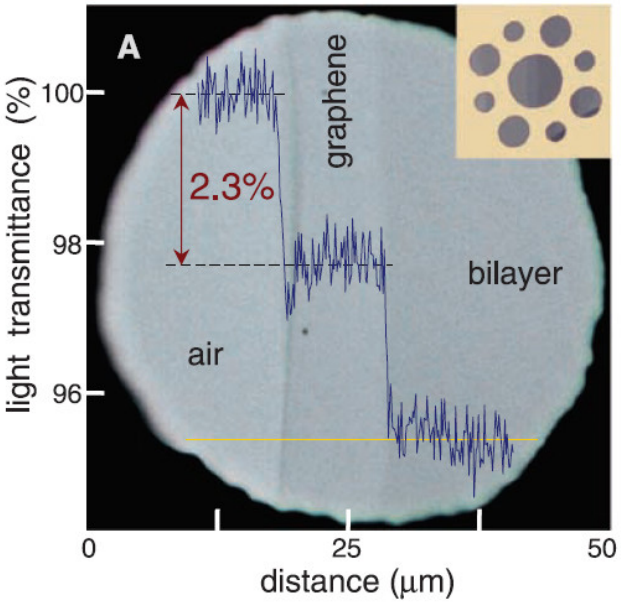

Figure 2.6: Experimental verification of graphene transmission. Reproduced from Ref. [26].

The energy carried by the electromagnetic radiation is $W_i = \frac{1}{2}c\epsilon_0 E_0^2$, where ϵ_0 is the perimittivity of vacuum. The transmission of the graphene layer is

$$T = 1 - \frac{W_a}{W_i} = 1 - \frac{e^2}{4\epsilon_0 \hbar c} = 1 - \pi\alpha. \tag{2.63}$$

Most surprisingly, the optical interband transition is not given by any material parameters. Instead, the transition is only given by the universal fine-structure constant $\alpha \approx 1/137$. And finally, this remarkable result was confirmed experimentally [115], as shown in Fig. 2.6.

2.3 Common Misconceptions

The graphene's unique properties, some of them shown above, attracted considerable interest in the scientific community. However, the missing detailed derivation of, e.g., pseudospin, Dirac Hamiltonian, or Landau levels sometimes led to a few misunderstandings. I will comment on the few most common misconceptions here.

2.3.1 Dirac or Schrödinger Equation

The first misconception is related to what Hamiltonian determines the motion of free charge carriers in graphene. Is it the Schrödinger equation, or is graphene so much different material that we have to use the Dirac equation? The answer should now be straightforward after we derived the graphene's electronic band structure in the previous section. The free electrons truly behave as in other materials, following the Schrödinger equation, as shown in Eq. (2.6). The Dirac equation is only a convenient approximation of the energy dispersion in the vicinity of the two K and K' points. This approximation roughly holds up ≈ 1 eV.

The trigonal warping starts playing the role for high energies, and the full band structure, not described by the Dirac hamiltonian, has to be taken into account for even higher energies. However, two touching Dirac cones have consequences similar to if the quasi-particles were relativistic. The Klein tunneling is the most pronounced effect representing the clear analogy with massless quasiparticles [23, 24].

2.3.2 Integer or Half-Integer Quantum Hall Effect?

The quantum Hall effect in graphene has different scaling apart from other metalic systems with parabolic dispersion. The filling factor ν determines quantization of the Hall resistance R_{xy} in parabolic bands as

$$R_{xy} = \frac{h}{e^2}\frac{1}{\nu}. \tag{2.64}$$

The spin-degenerated landau levels, indexed by the quantum number n, lead to $\nu = 2n$. Hence, we get

$$R_{xy} = \frac{h}{2e^2}\frac{1}{n}. \tag{2.65}$$

In graphene, the sequence of the filling factors is $\nu = \{2, 6, 10, 14, ...\}$, as shown in the previous section. Thus, the relation to the Landau level index n is $\nu = 2(2n + 1)$, and the resistance is quantized as

$$R_{xy} = \frac{h}{4e^2}\frac{1}{n + \frac{1}{2}}. \tag{2.66}$$

The factor $\frac{1}{2}$ in the denominator of (2.66) is the reason why the resistance quantization in graphene is sometimes called the half-integer quantum Hall effect. The inaccuracy is due to the impression of the fractional (1/2) states involved in this phenomenon. However, the filling factor is still integer here, $\nu = 2(2n + 1)$. The fractional quantum Hall effect requires fractional filling factors, at which new quasi-particles exist, so-called composite fermions. However, the resistance quantization in graphene is still a single particle phenomenon, where electrons (or holes) move in the disordered potential. Hence, it is more common to use expressions such as unusual or anomalous quantum Hall effect in graphene [35]. The reader should compare this Hall effect to the true fractional quantum Hall effect in graphene, observed experimentally, too [116, 117]. In this case, the composite fermions are really behind the experimental observation, and the true half-integer quantum Hall effect can be observed. The major requirement is the quality of graphene samples, namely the carrier mobility and the quantum lifetime.

2.3.3 Current Applications

The series of graphene's unique properties led to the possibility of a large number of potential applications. In fact, in the review work of Novoselov [118], the reader unfamiliar with the topic could get an impression that our whole world will be soon governed by graphene. We should already have graphene applications in touch screens, rollable e-paper, foldable organic light-emitting diodes, and tunable fiber mode-locked laser. A vast amount of applications should be

coming shortly, like a solid-state mode-locked laser, modulator, photodetector, polarization controller, high-frequency transistor, and logic thin-film transistor. None of these inventions exist today.
The touch screen, for example, is a standard part of our smartphones. However, the technology based on the indium tin oxide (ITO) is much more developed and reliable. Graphene does not seem to be competitive here in any sense. The reason is that the practical application in the touch screen technology has two major requirements. First, the material has to have good electrical conductivity. Second, it has to be optically transparent. Though graphene seems to fulfill both criteria, it fails in comparison with actual numbers. Applications to be competitive with ITO require a sheet resistance of at least 20 $\Omega/sq.$ and optical transparency of at least 95% [119]. Single-layer graphene has a typical resistivity higher. Hence, more than one layer is required. However, increasing the number of layers leads to reduced transparency. The optimum limit seems to be about four graphene layers. This factor will probably cause graphene never to be used as a touch screen apart from few experimental demonstrations.

Graphene as a non-linear material was largely criticized by Khurgin [120]. Khurgin argues that the material parameters determining the optical nonlinearities are all in the same range as in other materials (e.g., semiconductor quantum wells, organic semiconductors, or other 2D materials). Although there are also supporters of graphene as a non-linear material [121], it seems that further experimental rather than theoretical evidence will be required to resolve this question [122].

There is also a relatively big promotion of graphene in the popular scientific literature. Graphene is adored for its sports equipment applications (shoes, tennis rackets, bicycles), graphene printer powder, or as a new lubricant. These are typically mixed graphitic materials which, among others, also contain graphene sheets. Moreover, some of them, e.g. graphene as a lubricant, are graphite applications known and used for a long time. However, graphene is not used here for its intrinsic properties such as linear band structure, optical transparency, electrical conductivity, or anomalous quantum Hall effect.

On the other hand, probably the only application close to the realization is the resistance standard. Here, graphene indeed competes with current state-of-the-art GaAs-based quantum wells. The reason for this success is the large cyclotron gap. In SiC, the interface states between SiC and graphene also help to pin the Fermi level, and they cause a charge transfer, which further enlarges the quantum Hall plateaux, Fig. 2.7. This success is similar to many other successful technologies, like a transistor or giant magnetoresistance. All of them have one common denominator. It is the robustness of the effect. The transistor effect was realized on a piece of semiconductor contacted by a silver paste and gated through the water droplet and cat's whiskers. Giant magnetoresistance exhibits changes in the resistance by several orders of magnitude. This enormous effect stands behind the large storage capacity of today's hard drives. Such robustness is in contrast to, e.g., all-optical switching, which is a very bright idea for computation; however, the weakness of the effect is in the background of yet never realized commercial application. This is why graphene as a resistance standard is so successful. The Landau level quantization is a robust effect. The cyclotron resonance is much larger than in other known electron gasses, as compared in Fig. 2.5, and the

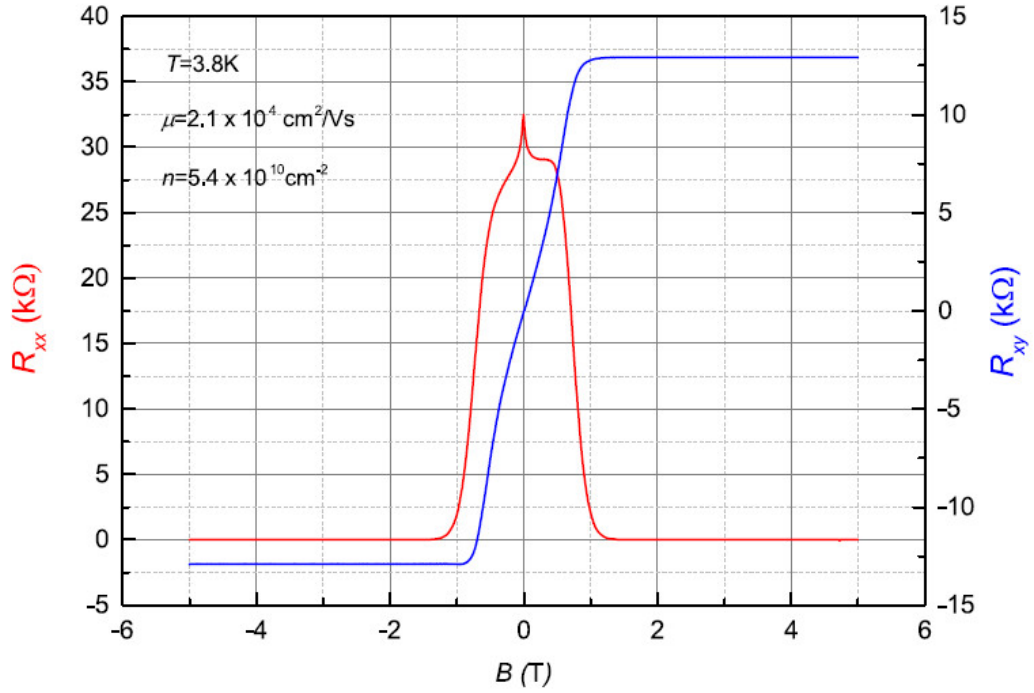

Figure 2.7: Quantum Hall effect in epitaxial graphene used in the resistance standard. (left) Longitudinal resistance and (right) Hall resistance show wide Hall plateaux at magnetic field well below 2 T and at 3.8 K. Reproduced from Ref. [123].

precision of the measured resistance is on the same level as in the conventional electron gas in GaAs quantum wells [106, 123]. Being the same would not be probably the reason for switching to graphene technology. Thanks to the large cyclotron gap, the same precision can be achieved at a lower magnetic field and higher temperature. That improvement greatly facilitates the instrumentation and reduces the cost of perpetual measurements of the resistance standard. Although this application is clearly on edge between applied science and industrial application, it is currently the most advanced graphene application.

Despite this critical view on the industrial application of graphene, there is still quite a broad range of promising applications. In my opinion, these are related to the strong absorption in the far-infrared and THz spectral range. Graphene as a channel for spin currents might be another such candidate. Generally, it is always hard to predict where any applications will evolve, and it is usually the least likely way the progress goes. It might not be the graphene's unique properties that will win the game; it might be the cost or ease of graphene production or any other neglected factor at this time.

Indeed, the graphene's boom can be compared to the boom of polymers in the 1970s, semiconductor quantum wells, plasmonics, carbon nanotubes, high-temperature superconductors, high T_C ferromagnetic semiconductors, and many others. These days the 2D transition metal chalcogenides and related materials are at their peak of interest, as well as perovskites for solar cells. Still, graphene remains an exciting material for its promising applications and unanswered fundamental physics questions.

2.3.4 Epitaxial Graphene and Rise of Epigraphene

The graphene grown by thermal decomposition of SiC is called epitaxial graphene. The term ”epitaxy” comes from Greek ”epi”, which means ”over” or ”upon”, and ”taxis” stands for ”order” [124]. The graphene on SiC is indeed an ordered carbon layer on top of the SiC monocrystalline substrate. The epitaxy is, therefore, a rational expression. However, the common understanding of ”epitaxy,” though not entirely correct itself [124], refers to the growth of oriented crystal on the crystal surface of the same (homoepitaxy) or different (heteroepitaxy) material. The epitaxial graphene on SiC is not grown by epitaxy in this commonly understood sense. Instead, the silicon sublimates at high temperatures, and the remaining carbon atoms form the graphene lattice from the initially SiC substrate itself. Hence, the epitaxial graphene layer is not deposited on the SiC substrate. However, this statement does not hold for the CVD graphene on SiC. The CVD graphene on SiC is the epitaxy in common sense. Due to such confusion, Walt de Heer proposed in 2018 at the 1^{st} Tianjin International Symposium on Epitaxial Graphene, Tianjin, China, that the graphene grown by thermal decomposition on SiC could be called ”epigraphene.” A. Tzalenchuk raised a worry about whether the term ”epigraphene” fulfills the formal scientific nomenclature requirements. Despite that, there are already some attempts using the name epigraphene [126, 3, 125].

3. Graphene Preparation

The graphene monolayer is a well-defined structure, and its properties are well-known from the theoretical point of view. When it comes to the experimental realization of graphene crystals, the possibilities open up, and the same holds for the properties of that given realization. As mentioned in the historical introduction, the first graphene was prepared on metal surfaces or transition metal carbides. However, such graphene is not very suitable for transport measurements. For this reason, a variety of methods were developed how the monolayer graphene can be prepared. Here I will briefly describe the most common methods, their advantages, and disadvantages.

3.1 Mechanical Exfoliation

The preparation of graphene layers was enormously demanding in the early days of the graphene boom after 2004. Such difficulties were probably the reason why mechanical exfoliation became so popular. The graphene can be obtained by using scotch tape and peeling few graphene layers from graphite. The graphite can be bought from various mining companies, or it can be a synthetic Highly Oriented Pyrolytic Graphite (HOPG). The scotch tape seems like a straightforward method to obtain graphene flakes. However, the yield is tiny. After the first peeling from the graphite crystal, the scotch tape has to be re-taped to itself many times until a homogeneous greyish layer of graphite flakes cover the tape. The tape is placed on top of the desired substrate, typically 300 nm of SiO_2 grown thermally on a silicon wafer. The tape is pressed to the substrate, removed, and the substrate is inspected under the microscope. The microscope reveals a large number of flakes of distinct optical contrast, differentiating the flakes' thickness. The areas of the lowest contrast are most likely graphene monolayers. Their occurrence is of about a few flakes per square centimeter. Although there are automated tools to identify these monolayers, the yield is still minimal. This method is undoubtedly inconsistent with an industrial needs of large-scale production. The advantage of the mechanical exfoliation is that it provides high-quality graphene. A further quality improvement can be achieved by encapsulating graphene into the boron nitride (BN) [127]. However, the complexity of such a manipulation is far from simple.

3.2 Graphene Flakes on Graphite

Probably the simplest way to obtain graphene is to fish for your luck on the graphite surface. Although transport measurements are prohibited here, optics can be the tool of choice. The graphite surface can occasionally have a decoupled graphene layers sitting loosely enough to exhibit graphene electronic band structure. These decoupled graphene layers might also be formed by the thermal stress while cooling the graphite sample from room to helium temperatures. Although this is only a speculation, the fact is that these decoupled graphene layers show unsurpassed carrier mobilities exceeding 10^7 cm^2/Vs [128]. Such high carrier mo-

bility has not been shown in any artificially made graphene until now. However, this experiment is, as the title of Neugebauer's paper states [128], a hallmark of how perfect can graphene be.

3.3 Chemical Vapor Deposition

Although the chemical vapor deposition (CVD) of graphene was known for a long time, the graphene quality was relatively poor in the early days of the graphene boom, though this statement holds somehow today [111]. Despite that, the highest quality CVD graphene growth rapidly accelerated, and from the perspective of the best achievements, it is the most serious competitor for the industrial application of graphene nowadays. The major issue in the high-quality CVD graphene is the complexity of the technological procedures. The growth requires a certain orientation of the metal seed. The grown graphene needs to be transferred by specialized methods in a clean environment. The device fabrication methods can be, besides others, also detrimental to graphene quality. The transfer is likely the most undefined process. The trapped water between graphene and the insulating substrate was found as one of several bottlenecks of CVD graphene [111]. A detailed investigation showed that the optimized process of growth, transfer, and measurements could provide graphene with mobility up to 12000 cm^2/Vs at room temperature on the Si/SiO_2 substrate [111]. The high uniformity and electron-hole symmetry was achieved as well. However, despite being one of the best CVD graphenes, the typical mobility still ranged from 5000 to 12000 cm^2/Vs. Encapsulation of CVD graphene in BN can enhance the mobility [129] similarly as in the case of mechanically exfoliated graphene. The recent work of Fazio [130] reported extraordinary $\approx$ 70 000 cm^2/Vs at room temperature and $\approx$ 120000 cm^2/Vs at 9 K. However, the reader should note here that the fabrication method of Fazio [130] is very similar to the mechanical exfoliation due to the exfoliation of BN flakes. Thus the high mobility is paid for by the lack of scalability.

3.4 Epitaxial Graphene on Silicon Carbide

The thermal decomposition of SiC is beside the CVD, one of the two most promising methods for the industrial growth of graphene. The main chamber of the furnace for epitaxial graphene growth, constructed by J. Kunc at the Institute of Physics, is shown in Fig. 3.1. The epitaxial graphene, or epigraphene, can be grown homogeneously in wafer-scale dimensions. The method is scalable, and currently, the only limitation of the scalability is the commercially available size of SiC substrates. The larges wafers available are 200 mm in diameter these days (II-VI Inc.). The SiC substrate's need is sometimes referred to as a disadvantage due to the wafer's high cost. The 4-inch wafer of the semi-insulating SiC on-axis wafer cost between \$1000 to \$2200, depending on the wafer production process, doping, resistivity, surface treatment, and other parameters. Considering a typical chip size of about 5×5 mm^2, and roughly 150 chips from one wafer (in the typical laboratory conditions), we arrive at the price \$15/chip. Although this price might seem too high, especially when compared to a similar chip made of

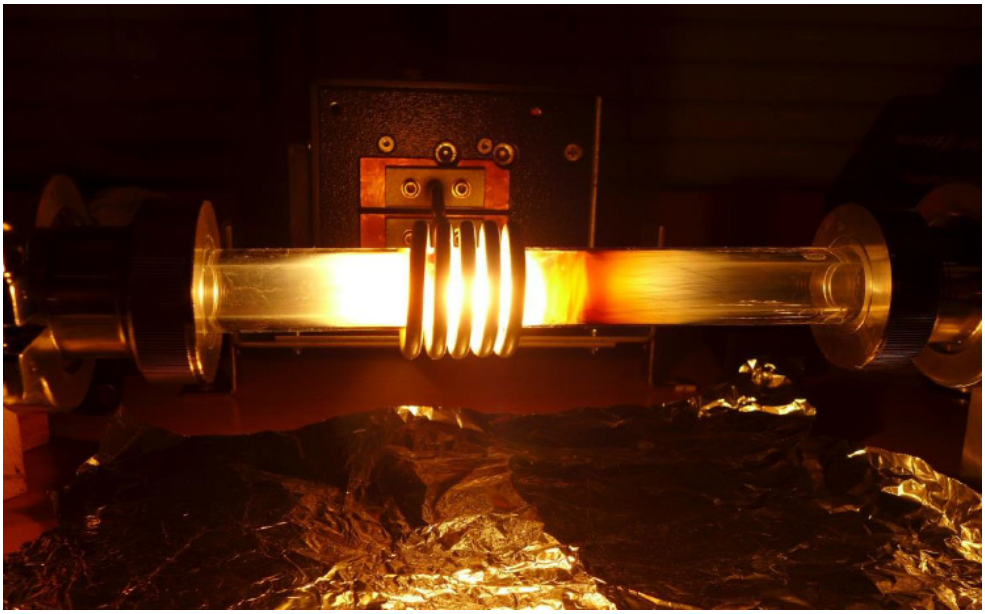

Figure 3.1: The main chamber of the induction furnace built at the Faculty of Mathematics and Physics for the growth of epitaxial graphene.

silicon, it is still reasonable concerning the possible applications. They are typically high-end niche applications where standard electronics fail. Such specialized applications can be priced higher. Thus the wafer cost is not the limiting factor. Moreover, the typical nanofabrication costs for the individual device are usually much higher, on hundreds to thousands of dollars per chip. However, this price can be greatly reduced by mass production.

Besides scalability, the electronic grade semi-insulating substrate brings another advantage. The semi-insulating substrate does not require any transfer of the grown graphene layer, as in CVD graphene. The SiC substrate plays a key role also in the eventual implementation of the technology to mass production. The reason is the CMOS-compatibility. Although this aspect is often overlooked, it is critical to decide whether it is worth replacing the silicon technology with the SiC one. The CMOS compatible nanofabrication means that the same nanofabrication facilities can be used as for silicon as for SiC. Hence, the entrance costs are significantly reduced.

One of the unique advantages of epitaxial graphene is that graphene can be formed into nanostructures without lithography. Fukidome demonstrated this property [131], and we further developed the idea with our Ph.D. student J. Palmer [4]. The work of J. Palmer was led under my supervision during my postdoctoral stay in the group of Walt de Heer.

Also, the SiC is known to be suitable for high-temperature, high-power applications. It is chemically inert, and it can resist large doses of radiation. The same holds for graphene. Thus the combination of SiC and graphene is a promising route for harsh environment applications like nuclear and chemical reactors, space, engine controls, and many others. Schlecht demonstrated such graphene-SiC device exploiting advantages of both. The graphene-SiC rectifier for THz radiation was successfully applied to study spectra of ethanol and acetone [132].

Besides advantages, there are also several issues which need to be resolved.

The major one is related to the advantage itself. The SiC substrate provides a magnificent platform for graphene. However, it also interacts with graphene at the same time. The interaction causes additional carrier scattering in graphene. Such scattering deteriorates carrier mobility to the order of $\approx$ 1000 cm^2/Vs for graphene grown on a Si face of SiC. It is worth noting that the mobility $\approx$ 1000 cm^2/Vs is not too far from about twice the carrier mobility in the SiC substrate. When we consider ideally terminated SiC and charge carriers moving on its surface, we can use the relaxation time approximation to calculate the scattering time on such an ideal surface. The relaxation time approximation requires calculation integrals over the whole reciprocal space. However, we need to integrate only over the half-space since we consider only the surface states now, and the scattering can happen only in the surface plane or towards the bulk. Most of the scattering mechanisms do not depend on the azimuthal angle. Thus the azimuthal scattering typically integrates to 2π. However, on the ideal surface, as we consider now, it integrates to π. Hence, it should be no surprise, applying the Mathiessen rule and considering that graphene's intrinsic mobility is several orders of magnitude larger than that of SiC, that the scattering mechanisms in SiC mainly determine the mobility of graphene on the surface of SiC. This effect of so-called remote scattering by the substrate phonons was identified by Jobst [89] experimentally. Another complication is related to the polar character of the SiC Si- and C-terminated surfaces. Hence, the phonons in SiC do not influence carriers in graphene only directly. They also produce an electric field that acts remotely and deteriorates charge mobility in graphene even further. Another possible mechanism of additional scattering is the trapped charge in the buffer layer.

The reduction of the SiC-graphene interaction is readily available by intercalation. The most common method is hydrogen intercalation. The hydrogen intercalation reduces the buffer layer and turns it into a graphene layer. This graphene layer is much further from the last layer of silicon atoms in SiC [134, 133]. Thus the interaction with substrate is reduced. The reduced interaction with substrate leads to a pronounced change in the temperature dependence of the carrier mobility [86]. The strong temperature dependence changes after intercalation to temperature-independent carrier mobility up to room temperature (3500 cm^{2}V^{-1}s^{-1} at 25 K, $\approx$ 3100 cm^{2}V^{-1}s^{-1} at 300 K). This observation indicates that the phonons do not play a major role anymore. The optimized hydrogen intercalation confirms the temperature-independent behavior, Tanabe [135], and shows mobility up to 4000 cm^{2}V^{-1}s^{-1} at 300 K.

Although it was experimentally determined by Jobst [89] that the resist residua and exposure to the ambient air does not influence the carrier mobility, the work of Yang [136] showed a significant improvement of carrier mobility when graphene was protected from the resist contamination by the gold layer during the nanofabrication steps. The gold doping of graphene might mostly cause this by shifting the Fermi level close to the Dirac point, where the carrier mobility is maximized. The typical carrier mobilities at 4 K were 4400-11000 cm^{2}V^{-1}s^{-1} for graphene grown on 6H-SiC, and 1640-6000 cm^{2}V^{-1}s^{-1} for graphene grown on 4H-SiC. The difference between polytypes might be related to the increased degree of hexagonality in 4H-SiC and correspondingly higher spontaneous polarization [137].

Another promising route to improve carrier mobility in epitaxial graphene is doping by tetrafluoro-tetracyanoquinodimethane (F4-TCNQ) [93]. The F4-TCNQ molecules are acceptors, and they deplete the high electron-doped graphene close to the Dirac point. Jobst showed mobility 29000 cm^2/Vs at $T = 25$ K, and about 2500 $cm^2V^{-1}s^{-1}$ at 300 K. The F4-TCNQ doping was further developed by He [110], showing mobility up to 70000 cm^2/Vs at 10 K. Despite decent mobilities, $2000 - 3000$ cm^2/Vs were reported at room temperature using the approach of sandwiched poly(methyl-methacrylate) and F4-TCNQ. Further improvements in the growth procedures were demonstrated by Kruskopf [109]. The so-called Polymer Assisted Sublimation Growth (PASG) helps growing homogenous single-layer graphene without bilayer islands with unprecedented reproducibility. Measurements show an electron mobility of 2800 cm^2/Vs at room temperature and 9500 cm^2/Vs at 2.2 K.

To summarize, the current state-of-the-art epitaxial graphene shows the best room temperature mobility about 4000 $cm^2V^{-1}s^{-1}$ [135], and the 4 K mobility on the order of 29000-70000 [93]. The best scalable CVD graphene seems to be slightly better with mobility 5000 $cm^2V^{-1}s^{-1}$ to 12000 cm^2/Vs at room temperature. However, as shown above, the significant improvements of epitaxial graphene are still in progress. The one-sided encapsulation of hydrogen intercalated graphene on SiC could be one way to enhance the carrier mobility even further.

3.5 Other Methods

There exist a plethora of other methods to grow graphene. For example, there is a nickel mediated catalytic decomposition of SiC at low temperatures [138] or a direct synthesis on SiO_2 [139]. The latter was motivated by no need for graphene transfer. However, the graphene quality was inferior in both cases.

Ruan demonstrated quite successful growth of graphene from the solid phase of carbon-rich materials [140]. The growth on the copper plate resulted in high-quality graphene. This result was even more surprising since the solid carbon sources were food, insects, and waste. Preparation of graphene by detonation [141] can be considered as another relatively obscure method.

4. Epitaxial Graphene Alloptropes

Graphene growth on SiC depends on the SiC polytype (4H, 6H, 3C, ...), surface orientation, and crystal miscut. The hexagonal polytypes show different sublimation dynamics [142]. Due to different decomposition energies of crystalographic steps in hexagonal polytypes, the so-called step bunching tends to keep the surface flat and regular even after graphene growth. Hence, from the perspective of regular and atomically flat terraces, the 6H polytype is the most favored for graphene growth. This prediction agrees with our experimental results. Indeed, the 4H polytype usually shows lower surface quality compared to the 6H polytype. The cubic 3C polytype does not show significant step bunching [142].

Graphene growth depends on the orientation of the SiC surface. The most common surfaces are the C-face SiC$(000\bar{1})$ and Si-face SiC(0001). There were attempts to grow graphene on a- and m-faces [143], although promising in reducing the charge transfer from the substrate, the results do not seem to provide too many advantages compared to the on-axis growth. Hence, I will focus on the on-axis growth on the C- and Si-face in the following paragraphs.

4.1 Graphene on C face of SiC

The graphene grows in the form of irregular islands of varying thickness on the SiC$(000\bar{1})$. The optical image in Fig. 4.1 shows areas of different brightness. These areas correspond to different graphene thicknesses. The graphene layers are typically rotated with respect to each other [59]. The rotational misalignment electronically decouples the layers, and they behave as single graphene sheets [144] clearly showing linear dispersion [145]. The decoupled nature of multilayers is why this graphene allotrope is called Multilayer Epitaxial Graphene (MEG). The growth of homogeneous single-layer graphene is difficult, and it usually grows only in the forms of isolated flakes. Lanzara [55] showed that about 25% of graphene

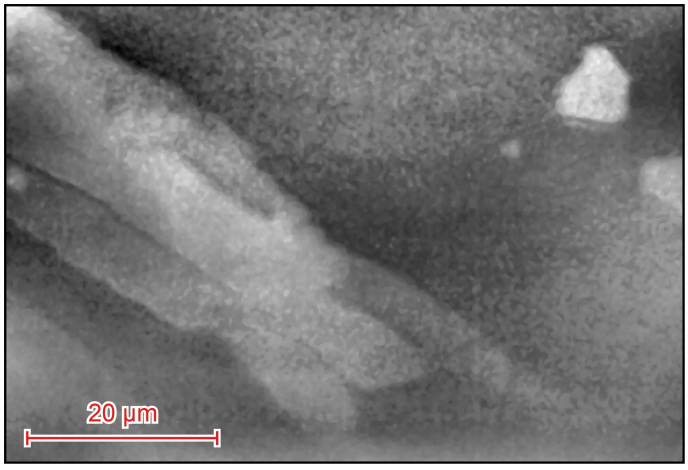

Figure 4.1: Optical micrograph of graphene grown on SiC$(000\bar{1})$.

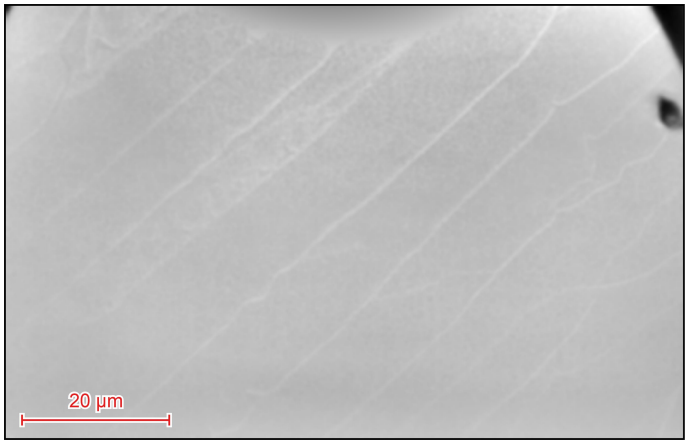

Figure 4.2: Optical micrograph of graphene grown on SiC(0001).

layers are AB stacked as in graphite. The MEG is also very lowly doped. The low doping is due to the short screening length of graphene [61].

4.2 Graphene on Si face of SiC

Graphene grown on SiC(0001) has lower carrier mobility than graphene on SiC($000\bar{1}$). However, the layer homogeneity is mostly improved, as shown in Fig. 4.2, where the wide flat terraces on 6H-SiC can be clearly seen. The fastest sublimation occurs at the edges of SiC terraces, where ribbons of bi-layers can be typically observed. These ribbons appear in Fig. 4.2 as narrow bright strips. These ribbons can be beneficial, as in side-wall graphene nanoribbons (SWGNR) [146]. However, the Polymer-Assisted Sublimation Growth (PASG) [109] can also reduce them if necessary.

Besides homogeneity, also a number of graphene layers can be relatively easily controlled. These are the two reasons why primary attention is paid to this kind of epitaxial graphene.

4.2.1 Buffer Layer

The first graphene-like layer grown on Si-face is the so-called buffer layer. The buffer layer consists of a hexagonal arrangement of carbon atoms as in the graphene lattice. However, about 30% of carbons are sp^3 bonded to the underlying silicon atoms in the SiC substrate [147]. The buffer layer has a different band structure than graphene, and it is more corrugated [133]. Riedl showed by Scanning Tunneling Microscopy (STM) and Low Energy Electron Diffraction (LEED) the $6\sqrt{3} \times 6\sqrt{3}$R30° reconstruction of the SiC(0001) surface with the buffer layer [148]. The tight-binding band structure is shown in Fig. 4.3. The simple tight-binding model describes the experimental data in Fig. 4.4 surprisingly well. The localized states in the bandgap can trap charges, or pin the Fermi energy, thus lowering carrier mobility in graphene layers above and prohibiting electrostatic gating [99]. The buffer layer grows at low temperatures 1300-1550°C, mainly depending on the growth conditions (argon, vacuum, ambient pressure, partial pressure). The exact temperature range for a given experimental setup

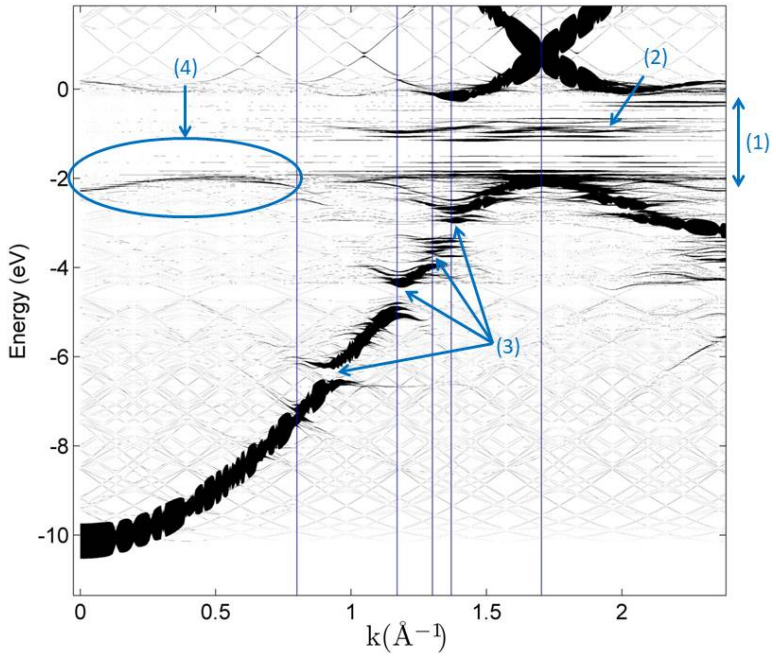

Figure 4.3: Tight-binding band structure of buffer layer. The $6\sqrt{3}\times 6\sqrt{3}R30°$ potential modulation explains all major experimentally observed feartures of buffer layer band structure, marked (1) ≈2 eV band gap, (2) localized states in the band gap, (3) set of four minigaps in the π-band, (4) slowly dispersing band at the Γ-point. (Unpublished calculation of J. Kunc)

typically provides a range of 20-30°C of homogeneous buffer growth.

4.2.2 Single-Layer Graphene

Upon increasing the growth temperature, silicon further sublimates, the buffer layer turns into graphene, and a new buffer layer forms at the SiC substrate interface and the newly formed graphene layer. The top graphene layer is highly doped due to the charge transfer from substrate [137]. The high electron density on the order of 10^{13} cm^{-2} is caused by the donor-like states at the SiC surface states and in the buffer layer. A small contribution originates from the doping of bulk SiC. The electron mobility is in the range 500-1200 cm^{2}V^{-1}s^{-1} at 300 K.

4.2.3 N-Layer Graphene

At even higher temperatures, the small islands of bi- and trilayers tend to grow. Mammadov reported growth of larger areas of these multilayers [149]. However, it is not an easy task to reach homogeneous layers. The significant difference to the MEG is that graphene on Si-face is mostly AB stacked as in graphite. This stacking leads to a different bandstructure, nearly identical to the graphite's bandstructure in a ten-layer AB stacked graphene.

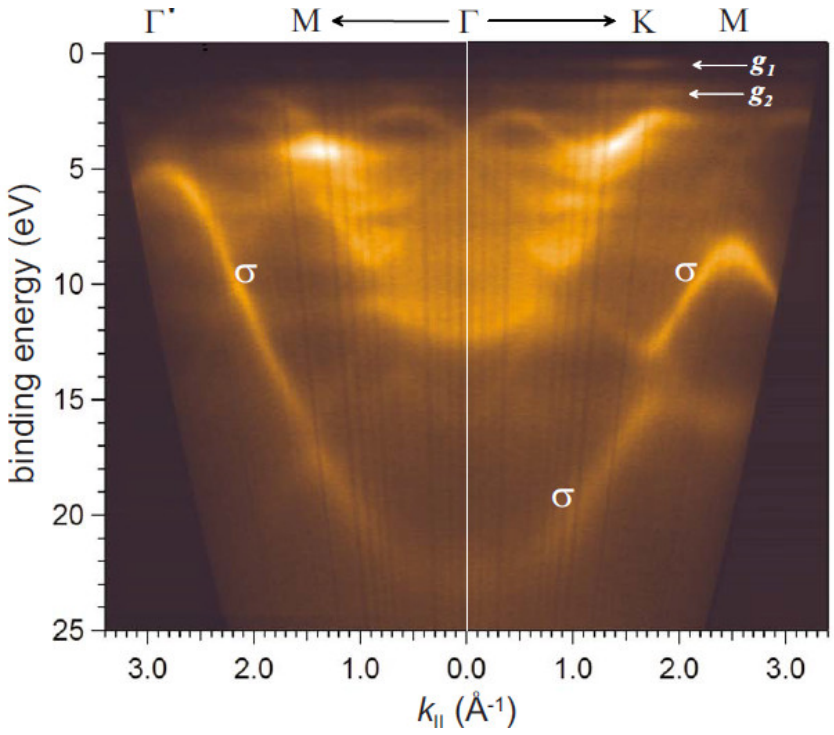

Figure 4.4: Experimentally determined band structure of the buffer layer. Reproduced from Ref. [147].

4.2.4 Quasi Free-Standing Monolayer Graphene

When buffer layer, the partially sp^3 bonded carbons, is annealed in hydrogen, the hydrogen saturates the silicon dangling bonds, and the sp^3 carbons hybridize to sp^2 [81]. Such a process is called hydrogen intercalation, and it results in high-quality monolayer graphene. Because this new graphene layer, formed from the buffer, is further from the SiC [134], the interaction with substrate is reduced. The graphene has a quasi-free-standing character, hence the name Quasi Free-standing Monolayer Graphene (QFMLG). The reduced interaction with substrate leads to increased and nearly temperature independent carrier mobility up to 300 K [86]. The graphene reaches p-type doping after full intercalation. The change from n-type to p-type is due to the dominant contribution of charge transfer from the buffer layer in non-intercalated graphene. The reduction of the buffer layer switches this charge transfer off. The remaining contribution is the fixed charge at the SiC surface resulting from the spontaneous polarization of hexagonal SiC polytypes [137]. This contribution is shadowed by the large density of localized interface states in single-layer graphene with the buffer layer.

4.2.5 Quasi Free-Standing Bilayer Graphene

Like QFMLG, hydrogen intercalation of the single-layer graphene leads again to the decoupling of the buffer layer from SiC. In this case, the Quasi Free-standing Bilayer Graphene (QFBLG) is formed. The QFBLG are two AB stacked graphene lattices with a unique band structure, different from single-layer graphene.

Generally, hydrogen intercalated graphene shows higher carrier mobility, and they are p-doped. The n-doping is observed in non-intercalated graphene or after

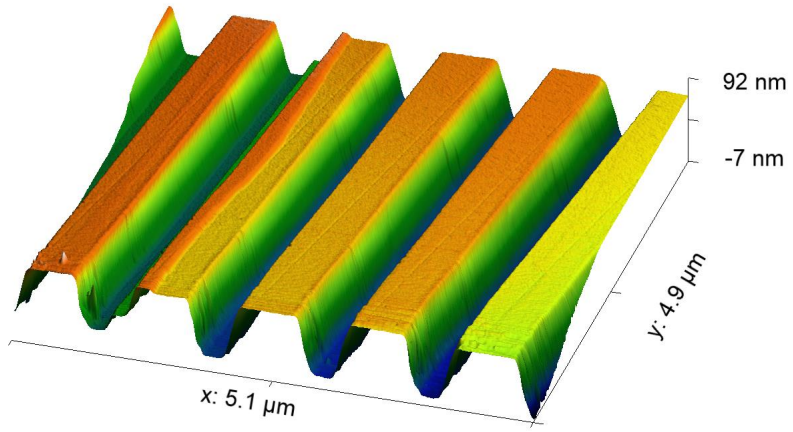

Figure 4.5: SiC trenches with side-wall graphene nanoribbons.

partial intercalation. The doping level is reduced with the increasing number of layers N, reaching the Dirac point in the limit of $N \to \infty$ [149].

4.3 Low-Dimensional Alloptropes of Epitaxial Graphene

Low dimensional structures fabricated from epitaxial graphene provide another extension of properties unseen in the two-dimensional lattice. Quantum confinement is the most pronounced effect. The lowered dimensionality also alters the electronic band structure in a rather non-trivial way. This phenomenon is the case of graphene nanoribbons cut along zig-zag direction [20]. The reduced dimension leads to the bandgap opening, the missing building block to incorporate graphene into digital electronics. The most promising applications of graphene nanoribbons (1D structures) and graphene quantum dots (0D structures) are described in the following section.

4.3.1 1-Dimensional Carbon World

The 1D nanostructures are commonly called nanowires. They are much longer than their radius. Though the cross-section does not have to be circular, the aspect ratio of the largest and the smallest width is on the order of one. Contrary to nanowires, graphene is atomically thin ($\approx 3\,\text{Å}$), and the typical width is at least a few nanometers (Hwang [150]), but more commonly 10's to 100's of nanometers. Hence, the two sizes are 10-1000× different. The shape thus resembles a ribbon instead of a wire. Therefore, the 1D graphene nanostructures are called graphene nanoribbons (GNR).

GNRs can be easily made by nanofabrication techniques, like photo- or electron-beam lithography. The drawbacks of such processing are the polymer

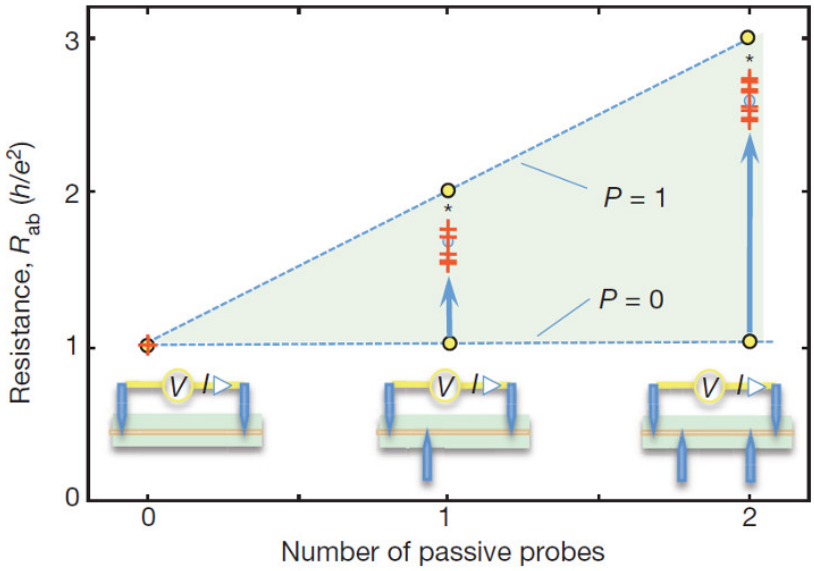

Figure 4.6: Experimental demonstration of the ballistic transport in side-wall graphene nanoribbons. Touching the ribbons leads to increased resistance by a resistance quantum. Reproduced from Ref. [152].

residua (e-beam or photoresist), which are difficult to be entirely removed, and rough edges. The rough edges are inevitable after plasma etching treatment, which is also a part of the nanofabrication process. The advantage of epitaxial graphene is its SiC substrate. The silicon sublimation rate depends on the crystallographic facet of SiC. This property can be used to fabricate so-called side-wall graphene nanoribbons (SWGNR). When the SiC surface, oriented in a (0001) direction, is etched through a desired mask, the subsequent annealing leads to a prior sublimation from the non-(0001) facets, where graphene nanoribbons form first. These SWGNRs are shown in Fig. 4.5. The SWGNRs solve both problems of directly made ribbons. Resist residua do not contaminate them, and they are well-terminated into the SiC substrate without too rough edges. These advantages led to the emergence of unique ballistic channels [152, 151].

Ballistic channels conduct electrical current without losses. The lossless signal transmission is undoubtedly a technologically appealing property, especially when we consider that most of today's electronics' power consumption is due to losses via Joule heat. Ballistic channels are also fascinating systems for testing fundamental physics. It would be rather unusual thinking that a piece of copper wire changes its resistance when we touch it. The measured resistance can change due to leakage currents. However, this is a systematic error of the measurements. In the ballistic wires, the situation is different. Touching the ballistic wire, the resistance changes, and the change is not a systematic error. The resistance change will occur even if the touching point is not grounded. As the theory predicts, the resistance changes by a resistance quantum $h/e^2 = 25818$ kΩ, also called the Klitzing constant. The reason is that each ballistic channel has a length-independent conductance e^2/h. Thus, touching the ballistic wire means that we split one ballistic channel into two; therefore, the resistance doubles. Further on, when touching the wire at two points, the resistance triples. The result of this

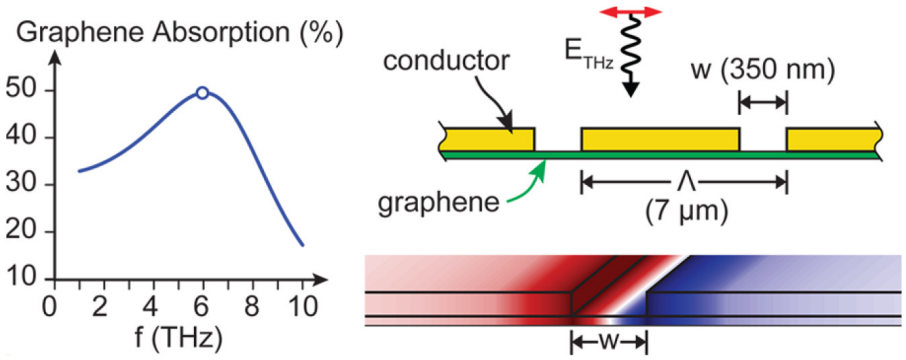

Figure 4.7: (left) Plasmon resonance in graphene nanoribbons in the terahertz spectral range. (right top) Geometry of metal antennas used to excite plasmonic excitations in graphene. (right bottom) Electric field distribution inside the metal gap. Reproduced from Ref. [153].

experiment is shown in Fig. 4.6.

Another unique property of graphene nanoribbons is their ability to absorb up to 50% of incoming light. Such absorption is in far contrast to ≈ 2.6 % of pristine interband graphene absorption. Here, the absorption is due to the strong light-matter interaction and absorption by plasma oscillations. Unfortunately, the plasmons cannot be excited in pristine graphene because the plasmon's dispersion does not intersect the dispersion of light. Hence the momentum conservation is not fulfilled. The momentum matching can be reached when light propagates from the medium with an index of refraction $n > 1$; this is the so-called Otto configuration. Another option is to gain momentum by a grating. Hence, an array of graphene ribbons is an excellent platform for strong light-matter coupling in GNRs. When such a grating is made of gold, as shown in Fig. 4.7, the absorption reaches the claimed 50% [153].

Because ballistic channels and plasmons in GNRs and SWGNRs are perspective graphene nanostructures, they are in the scope of our current intensive research interest. This topic combines all aspects of modern physics, such as quantum physics, light-matter interaction, and nanotechnology.

4.3.2 0-Dimensional Carbon World

Reducing dimension even further leads us to the zero-dimensional nanostructures, or, sometimes called artificial atoms/molecules, or quantum dots. The smallest graphene quantum dot is a benzene molecule. Benzene molecules are well-known species. However, contacting a molecule by wires and measuring a current through, or using the molecule as a detector, are the challenges faced by state-of-the-art science. Indeed, graphene junctions were used by Ullmann [154] to measure current-voltage characteristics of single fullerene-like molecules. Ullmann also showed that the graphene contacts are better than the metallic contacts because there is easier access by experimental probes (Scanning Tunneling Spectroscopy probes, optical access) to the molecular junction.

A different approach is to fabricate a real graphene quantum dot by electron-beam lithography and use such a dot as a detector. Such dots were shown by

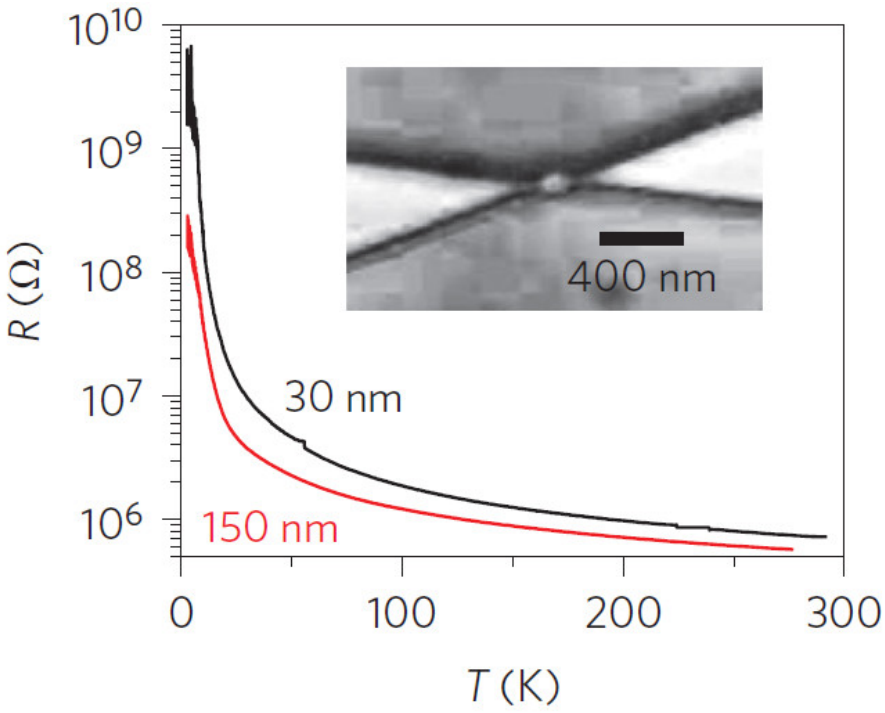

Figure 4.8: Graphene quantum dot bolometer. Reproduced from Ref. [155].

Fatimy [156] to be excellent bolometers. The highest efficiency was achieved for 30 nm small quantum dots where the highest temperature dependence of the resistance was observed, as shown in Fig. 4.8. The main drawback is the need for large antennas. They restrict the spectral bandwidth, and they also reduce the filling factor of the active detector area.

It should be now apparent from this brief introduction that graphene nanostructures are exciting condensed matter systems. Regardless of dimension, many new optical, transport, and optoelectronic properties emerged. Technologically attractive high absorption in gold excited graphene plasmons, graphene bolometers, or understanding ballistic channels in SWGNRs stimulates our further understanding of physics's fundamental laws and promotes nanotechnology progress. Undoubtedly, further progress in this research field has a great promise to change and improve our whole society's well-being.

5. Author's Contributions

5.1 Graphene

The paper "Planar Edge Schottky Barrier-Tunneling Transistors Using Epitaxial Graphene/SiC Junctions" [5] was one of my main works during my postdoctoral stay at the Georgia Insitute of Technology, Atlanta, USA. I analyzed experimental data, and I proposed a theoretical model. I did numerical simulations and co-wrote the manuscript.

The paper "A method to extract pure Raman spectrum of epitaxial graphene on SiC" [6] (corresponding author) came from my long-standing idea to apply a new numerical method, so-called Non-negative Matrix Factorization. This method is similar to the Singular Value Decomposition. However, it decomposes the input vectors into the non-negative basis functions. This condition is much more natural in physics because merged signals usually add up (if interference is negligible). I conducted the experiments, data analysis, interpretation, and I wrote the manuscript.

The work "A wide-bandgap metal-semiconductor-metal nanostructure made entirely from graphene" [7] was published in Nature Physics. I modeled the experimental data numerically. I came with the theoretical model and implemented the Matlab code to solve the tight-binding band structure of graphene ribbons, and I fitted the model to experimental data.

The work "Controlled epitaxial graphene growth within removable amorphous carbon corrals" [4] was supervised by me during my postdoctoral stay in Atlanta. The first author, James Palmer, was a Ph.D. student who did most of the work. I also contributed to few verification experiments. We showed that step bunching on SiC could be governed by artificial structures made of amorphous carbon.

The work "Effect of Residual Gas Composition on Epitaxial Growth of Graphene on SiC" [1] (corresponding author) was the first work in our graphene group in Prague, which I have established after the return from my postdoc position in the USA. We studied differences of vacuum-grown and argon-grown graphene and the residual gas influence on graphene's quality. We found that the residual gases cause a variety of chemical reactions that might deteriorate the graphene growth. We pointed out the importance of using ultra-high purity gases, including on-site purification.

The second work of our Prague's group was "Hydrogen intercalation of epitaxial graphene and buffer layer probed by mid-infrared absorption and Raman spectroscopy" [8] (corresponding author), where we investigated methods of hydrogen intercalation and temporal stability of hydrogen intercalated graphene.

We investigated electroluminescent properties of SiC in combination with graphene in "The electroluminescent properties based on bias polarity of the epitaxial graphene/aluminium SiC junction" [9]. We identified different optical transitions involved in the forward and reversed bias polarity of the graphene-SiC junction. We also found the Franz-Keldysh effect of band gap variation with the external electric field.

We discovered a new phonon mode in "ZO phonon of a buffer layer and Raman mapping of hydrogenated buffer on SiC(0001)" [10]. We attributed the new

phonon mode to the ZO phonon of the buffer layer. We also studied homogeneity and strain variations of hydrogen intercalated graphene.

We developed a new characterization technique of SiC homoepitaxy in "Thickness of sublimation grown SiC layers measured by scanning Raman spectroscopy" [2] (corresponding author). The method is based on the Raman spectroscopy of coupled plasmon-LO phonon in SiC. We also presented the growth of thin vanadium doped SiC on nitrogen-doped SiC monocrystals. We showed that high-quality graphene could be grown on as-grown layers in the stoichiometric vapors of SiC. We showed that the stoichiometric vapors could be realized by admixing hydrogen in the argon ambient. The hydrogen reacts with carbon, forming hydrocarbons, thus enhancing the carbon concentration in the vapor phase.

"Contactless millimeter-wave method for quality assessment of large area graphene" [11] was done as a part of my collaboration with Dr. Dominik Bloos and Dr. Petr Neugebauer in the group of prof. Joris van Slageren at the University of Stuttgart, Germany. I proposed a theoretical model to analyze the experimental data, and I analyzed the data together with Dr. Bloos. We wrote the manuscript together.

The work "Raman 2D Peak Line Shape in Epigraphene on SiC" [3] (corresponding author) was motivated by the ever observed differences in the line shape of argon-grown and hydrogen-intercalated samples. The argon-grown samples typically show signatures of the Lorentzian line shape, as predicted by theory. However, the Lorentzian line shape in hydrogen intercalated samples is always much more pronounced. My idea was to investigate the real line shape of Raman 2D peak in graphene. I found that the lineshape is better described by the convolution of the Lorentzian and Gaussian broadening. While the Lorentzian broadening is related to the intrinsic lifetime, the Gaussian broadening is related to the inhomogeneity. In the case of 2D peak, the inhomogeneity is given mainly by strain fluctuations on the nanometer length scale. The inhomogeneous broadening described by the Gauss part of the convolution is much more pronounced in the argon-grown samples.

My former Ph.D. student RNDr. Vojtěch Vozda, Ph.D. investigated "Detachment of epitaxial graphene from SiC substrate by XUV laser radiation" [12] under my supervision. I led this project from the beginning, and I significantly helped with data analysis and several experiments. We found that graphene is detached by XUV radiation from the SiC substrate without significant deterioration of its lattice. We determined the XUV intensity range of these processes, and we found that this process is possible due to the mutually fitted damage thresholds of graphene and SiC.

5.2 Other topics

Besides my primary interest in epitaxial graphene, I also investigated magneto-optical and magneto-transport properties of a two-dimensional electron gas in CdTe quantum wells during my Ph.D. study. The two leading publications are "Enhancement of the spin gap in fully occupied two-dimensional Landau levels" [13] (corresponding author) and "Magnetoresistance quantum oscillations in a magnetic two-dimensional electron gas" [14] (corresponding author) where I did most of the experimental work, data analysis, interpretation, and data modeling.

The work ref. [14] was selected as Editors' Suggestion in Physical Review B.

Currently, I am also partially involved in the study of CdTe bulk radiation detectors. I developed a theory to explain data of the Transient Current Technique. I proposed and implemented a two-dimensional model that realistically described all current transients in our radiation detectors. I summarized the results of my numerical simulations in the publication "Efficient Charge Collection in Coplanar-Grid Radiation Detectors" [15] (corresponding author).

Selected Author's Publications

[1] J. Kunc, M. Rejhon, E. Belas, V. Dedic, P. Moravec, and J. Franc. Effect of residual gas composition on epitaxial growth of graphene on sic. *Physical Review Applied*, 8(4):044011, 2017. DOI: 10.1103/PhysRevApplied.8.044011.

[2] J. Kunc, M. Rejhon, V. Dedic, and P. Babor. Thickness of sublimation grown sic layers measured by scanning raman spectroscopy. *Journal of Alloys and Compounds*, 789:607–612, 2019. DOI: 10.1016/j.jallcom.2019.02.305.

[3] Jan Kunc and Martin Rejhon. Raman 2d peak line shape in epigraphene on sic. *Applied Sciences-Basel*, 10(7):2354, 2020. DOI: 10.3390/app10072354.

[4] James Palmer, Jan Kunc, Yike Hu, John Hankinson, Zelei Guo, Claire Berger, and Walt A. de Heer. Controlled epitaxial graphene growth within removable amorphous carbon corrals. *Applied Physics Letters*, 105(2):023106, 2014. DOI: 10.1063/1.4890499.

[5] Jan Kunc, Yike Hu, James Palmer, Zelei Guo, John Hankinson, Salah H. Gamal, Claire Berger, and Walt A. de Heer. Planar edge schottky barrier-tunneling transistors using epitaxial graphene/sic junctions. *Nano Letters*, 14(9):5170–5175, 2014. DOI: 10.1021/nl502069d.

[6] J. Kunc, Y. Hu, J. Palmer, C. Berger, and W. A. de Heer. A method to extract pure raman spectrum of epitaxial graphene on sic. *Applied Physics Letters*, 103(20):201911, 2013. DOI: 10.1063/1.4830374.

[7] J. Hicks, A. Tejeda, A. Taleb-Ibrahimi, M. S. Nevius, F. Wang, K. Shepperd, J. Palmer, F. Bertran, P. Le Fevre, J. Kunc, W. A. de Heer, C. Berger, and E. H. Conrad. A wide-bandgap metal-semiconductor-metal nanostructure made entirely from graphene. *Nature Physics*, 9(1):49–54, 2013. DOI: 10.1038/NPHYS2487.

[8] J. Kunc, M. Rejhon, and P. Hlidek. Hydrogen intercalation of epitaxial graphene and buffer layer probed by mid-infrared absorption and raman spectroscopy. *AIP Advances*, 8(4):045015, 2018. DOI: 10.1063/1.5024132.

[9] M. Rejhon, J. Franc, V. Dedic, P. Hlidek, and J. Kunc. The electroluminescent properties based on bias polarity of the epitaxial graphene/aluminium sic junction. *Journal of Physics D-Applied Physics*, 51(26):265104, 2018. DOI: 10.1088/1361-6463/aac7d2.

[10] Martin Rejhon and Jan Kunc. Zo phonon of a buffer layer and raman mapping of hydrogenated buffer on sic(0001). *Journal of Raman Spectroscopy*, 50(3):465–473, 2019. DOI: 10.1002/jrs.5533.

[11] D. Bloos, J. Kunc, L. Kaeswurm, R. L. Myers-Ward, K. Daniels, M. DeJarld, A. Nath, J. van Slageren, D. K. Gaskill, and P. Neugebauer. Contactless millimeter wave method for quality assessment of large area graphene. *2D Materials*, 6(3):035028, 2019. DOI: 10.1088/2053-1583/ab1d7e.

[12] V. Vozda, N. Medvedev, J. Chalupsky, J. Cechal, T. Burian, V Hajkova, L. Juha, M. Krus, and J. Kunc. Detachment of epitaxial graphene from sic substrate by xuv laser radiation. *Carbon*, 161:36–43, 2020. DOI: 10.1016/j.carbon.2020.01.028.

[13] J. Kunc, K. Kowalik, F. J. Teran, P. Plochocka, B. A. Piot, D. K. Maude, M. Potemski, V. Kolkovsky, G. Karczewski, and T. Wojtowicz. Enhancement of the spin gap in fully occupied two-dimensional landau levels. *Physical Review B*, 82(11):115438, 2010. DOI: 10.1103/PhysRevB.82.115438.

[14] J. Kunc, B. A. Piot, D. K. Maude, M. Potemski, R. Grill, C. Betthausen, D. Weiss, V. Kolkovsky, G. Karczewski, and T. Wojtowicz. Magnetoresistance quantum oscillations in a magnetic two-dimensional electron gas. *Physical Review B*, 92(8):085304, 2015. DOI: 10.1103/PhysRevB.92.085304.

[15] J. Kunc, P. Praus, E. Belas, V. Dedic, J. Pekarek, and R. Grill. Efficient charge collection in coplanar-grid radiation detectors. *Physical Review Applied*, 9(5):054020, 2018. DOI: 10.1103/PhysRevApplied.9.054020.

Conclusion

This work aimed to present a brief history of graphene, its basic electronic and optical properties, methods of preparation, types of epitaxial graphene, differences of graphene growth on C-face and Si-face of SiC, different SiC polytypes, and to present novel routes in graphene research towards one and zero dimension nanostructures.

I showed that the history of graphene started a long time before 2004. Graphite monolayers were studied intensively in the 1990s, and they were stable monolayers on various substrates. I showed that graphene is not one. There are many types of graphene, depending on how we prepare this two-dimensional crystal. Neither the epitaxial graphene is one. There is multi-layer epitaxial graphene on C-face, buffer layer, single layer with buffer, quasi free-standing monolayers, or quasi free-standing bilayer. They all provide a rich variability for many experiments in demand. I showed few misconceptions, such as the true origin of the Dirac hamiltonian, unusual quantum Hall effect, nomenclature of epitaxial graphene, or claimed applications of graphene.

Although it might seem from the number of publications that the field must be entirely exploited, the truth is different. Particularly for the case of epitaxial graphene, the field seems to have matured in the last ten years. This progress is a characteristic of each new technology described by Gartner's hype curve. The first wave of excessive interest in graphene has passed. The thru of disillusionment as well. We already know most of the pros and cons of graphene, and the progress has no significant unrealistic expectations, apart from the early years of the graphene boom right after 2004.

And last but not least. I could extend the statement from above. Graphene is not one, and graphene is not the only one. There are currently many other two-dimensional crystals that emerged recently. The transition metal dichalcogenides (TMD), boron nitride, topological insulators, Weyl semimetals, nodal line semimetals, the selection is enormous.

In my opinion, though all of them are interesting from the fundamental physics' point of view, they usually seem to possess at least one serious drawback. The TMDs have poor carrier mobility, typically reaching the values of poor-quality graphene crystals. Though they often have a bandgap, the most promising studies are optical experiments due to the low mobility. Boron nitride is hard to prepare in large homogeneous layers. Topological insulators are not stable in the air. Technological progress typically builds on robustness. We can grow ultrapure silicon ingots because it is relatively easy to purify a monoatomic crystal. We were able to dramatically increase the hard-drives' capacity because the giant magnetoresistance is a robust effect. The wireless transmission can be demonstrated in the practical courses using simple electronic equipment. Alternatively, as mentioned earlier, the transistor effect can be demonstrated by a simple table-top experiment. Thus, I believe that the resistance standard, due to the robustness of the quantum Hall effect in graphene, is the nearest-future graphene commercialization. The graphene plasmonic nanostructures, for their enormous and robust absorbance in far-infrared, are, in my opinion, the second candidate for such a transition from fundamental research to industry. Though

the predictions are always difficult, what is for granted, we will not lack surprises on our way to that goal.

Bibliography

[16] KS Novoselov, AK Geim, SV Morozov, D Jiang, Y Zhang, SV Dubonos, IV Grigorieva, and AA Firsov. Electric field effect in atomically thin carbon films. *Science*, 306(5696):666–669, 2004. DOI: 10.1126/science.1102896.

[17] C Berger, ZM Song, TB Li, XB Li, AY Ogbazghi, R Feng, ZT Dai, AN Marchenkov, EH Conrad, PN First, and WA de Heer. Ultrathin epitaxial graphite: 2d electron gas properties and a route toward graphene-based nanoelectronics. *Journal of Physical Chemistry B*, 108(52):19912–19916, 2004. DOI: 10.1021/jp040650f.

[18] YB Zhang, YW Tan, HL Stormer, and P Kim. Experimental observation of the quantum hall effect and berry's phase in graphene. *Nature*, 438(7065):201–204, 2005. DOI: 10.1038/nature04235.

[19] A. K. Geim. Graphene prehistory. *Physica Scripta*, T146:014003, 2012. DOI: 10.1088/0031-8949/2012/T146/014003. Nobel Symposium on Graphene and Quantum Matter, Saltsjobaden, SWEDEN, MAY 27-31, 2010.

[20] K Wakabayashi, M Fujita, H Ajiki, and M Sigrist. Electronic and magnetic properties of nanographite ribbons. *Physical Review B*, 59(12):8271–8282, 1999. DOI: 10.1103/PhysRevB.59.8271.

[21] KS Novoselov, AK Geim, SV Morozov, D Jiang, MI Katsnelson, IV Grigorieva, SV Dubonos, and AA Firsov. Two-dimensional gas of massless dirac fermions in graphene. *Nature*, 438(7065):197–200, 2005. DOI: 10.1038/nature04233.

[22] YB Zhang, JP Small, WV Pontius, and P Kim. Fabrication and electric-field-dependent transport measurements of mesoscopic graphite devices. *Applied Physics Letters*, 86(7):073104, 2005. DOI: 10.1063/1.1862334.

[23] M. I. Katsnelson, K. S. Novoselov, and A. K. Geim. Chiral tunnelling and the klein paradox in graphene. *Nature Physics*, 2(9):620–625, 2006. DOI: 10.1038/nphys384.

[24] Andrea F. Young and Philip Kim. Quantum interference and klein tunnelling in graphene heterojunctions. *Nature Physics*, 5(3):222–226, 2009. DOI: 10.1038/NPHYS1198.

[25] KS Novoselov, D Jiang, F Schedin, TJ Booth, VV Khotkevich, SV Morozov, and AK Geim. Two-dimensional atomic crystals. *Proceedings of the National Academy of Sciences of the United States of America*, 102(30):10451–10453, 2005. DOI: 10.1073/pnas.0502848102.

[26] R. R. Nair, P. Blake, A. N. Grigorenko, K. S. Novoselov, T. J. Booth, T. Stauber, N. M. R. Peres, and A. K. Geim. Fine structure constant defines visual transparency of graphene. *Science*, 320(5881):1308, 2008. DOI: 10.1126/science.1156965.

[27] NR Gall, EV RutKov, and AY Tontegode. Two dimensional graphite films on metals and their intercalation. *International Journal of Modern Physics B*, 11(16):1865–1911, 1997. DOI: 10.1142/S0217979297000976.

[28] C Oshima and A Nagashima. Ultra-thin epitaxial films of graphite and hexagonal boron nitride on solid surfaces. *Journal of Physics-Condensed Matter*, 9(1):1–20, 1997. ISSN: 0953-8984. DOI: 10.1088/0953-8984/9/1/004.

[29] H. P. Boehm, R. Setton, and E. Stumpp. Nomenclature and terminology of graphite-intercalation compounds-report by a subgroup of the international comittee for characterization and terminology of carbon and graphite on suggestions for rules for the nomenclature and terminology of graphite-intercalation compounds. *Synthetic Metals*, 11(6):363–371, 1985. DOI: 10.1016/0379-6779(85)90068-2.

[30] T Takahashi, H Tokailin, and T Sagawa. Angle-resolved ultraviolet photoelectron-spectroscopy of the unoccupied band-structure of graphite. *Physical Review B*, 32(12):8317–8324, 1985. ISSN: 1098-0121. DOI: 10.1103/PhysRevB.32.8317.

[31] XK Lu, MF Yu, H Huang, and RS Ruoff. Tailoring graphite with the goal of achieving single sheets. *Nanotechnology*, 10(3):269–272, 1999. DOI: 10.1088/0957-4484/10/3/308. 6th Foresight Conference, SANTA CLARA, CALIFORNIA, NOV 12-15, 1998.

[32] B. C. Brodie. *Phil. Trans. R. Soc. A*, 149:249, 1859.

[33] A.J. Van Bommel, J.E. Crombeen, and A. Van Tooren. Leed and auger electron observations of the sic(0001) surface. *Surface Science*, 48(2):463–472, 1975. ISSN: 0039-6028. DOI: https://doi.org/10.1016/0039-6028(75)90419-7.

[34] I Forbeaux, JM Themlin, and JM Debever. Heteroepitaxial graphite on 6h-sic(0001): interface formation through conduction-band electronic structure. *Physical Review B*, 58(24):16396–16406, 1998. DOI: 10.1103/PhysRevB.58.16396.

[35] A. H. Castro Neto, F. Guinea, N. M. R. Peres, K. S. Novoselov, and A. K. Geim. The electronic properties of graphene. *Reviews of Modern Physics*, 81(1):109–162, 2009. DOI: 10.1103/RevModPhys.81.109.

[36] Andrea C. Ferrari. Raman spectroscopy of graphene and graphite: disorder, electron-phonon coupling, doping and nonadiabatic effects. *Solid State Communications*, 143(1-2):47–57, 2007. DOI: 10.1016/j.ssc.2007.03.052.

[37] F. Bonaccorso, Z. Sun, T. Hasan, and A. C. Ferrari. Graphene photonics and optoelectronics. *Nature Photonics*, 4(9):611–622, 2010. DOI: 10.1038/NPHOTON.2010.186.

[38] Daniel R. Dreyer, Sungjin Park, Christopher W. Bielawski, and Rodney S. Ruoff. The chemistry of graphene oxide. *Chemical Society Reviews*, 39(1):228–240, 2010. DOI: 10.1039/b917103g.

[39] Frank Schwierz. Graphene transistors. *Nature Nanotechnology*, 5(7):487–496, 2010. DOI: 10.1038/NNANO.2010.89.

[40] Vasilios Georgakilas, Michal Otyepka, Athanasios B. Bourlinos, Vimlesh Chandra, Namdong Kim, K. Christian Kemp, Pavel Hobza, Radek Zboril, and Kwang S. Kim. Functionalization of graphene: covalent and non-covalent approaches, derivatives and applications. *Chemical Reviews*, 112(11):6156–6214, 2012. DOI: 10.1021/cr3000412.

[41] Xiao Huang, Xiaoying Qi, Freddy Boey, and Hua Zhang. Graphene-based composites. *Chemical Society Reviews*, 41(2):666–686, 2012. DOI: 10.1039/c1cs15078b.

[42] Alexander A. Balandin. Thermal properties of graphene and nanostructured carbon materials. *Nature Materials*, 10(8):569–581, 2011. DOI: 10.1038/NMAT3064.

[43] F. H. L. Koppens, T. Mueller, Ph. Avouris, A. C. Ferrari, M. S. Vitiello, and M. Polini. Photodetectors based on graphene, other two-dimensional materials and hybrid systems. *Nature Nanotechnology*, 9(10):780–793, 2014. DOI: 10.1038/NNANO.2014.215.

[44] Tony Low and Phaedon Avouris. Graphene plasmonics for terahertz to mid-infrared applications. *ACS Nano*, 8(2):1086–1101, 2014. DOI: 10.1021/nn406627u.

[45] Qiaoliang Bao and Kian Ping Loh. Graphene photonics, plasmonics, and broadband optoelectronic devices. *ACS Nano*, 6(5):3677–3694, 2012. DOI: 10.1021/nn300989g.

[46] A. N. Grigorenko, M. Polini, and K. S. Novoselov. Graphene plasmonics. *Nature Photonics*, 6(11):749–758, 2012. DOI: 10.1038/NPHOTON.2012.262.

[47] Florian Banhart, Jani Kotakoski, and Arkady V. Krasheninnikov. Structural defects in graphene. *ACS Nano*, 5(1):26–41, 2011. DOI: 10.1021/nn102598m.

[48] Yuyan Shao, Jun Wang, Hong Wu, Jun Liu, Ilhan A. Aksay, and Yuehe Lin. Graphene based electrochemical sensors and biosensors: a review. *Electroanalysis*, 22(10):1027–1036, 2010. DOI: 10.1002/elan.200900571.

[49] David S. Hecht, Liangbing Hu, and Glen Irvin. Emerging transparent electrodes based on thin films of carbon nanotubes, graphene, and metallic nanostructures. *Advanced Materials*, 23(13):1482–1513, 2011. DOI: 10.1002/adma.201003188.

[50] Yi Huang, Jiajie Liang, and Yongsheng Chen. An overview of the applications of graphene-based materials in supercapacitors. *Small*, 8(12):1805–1834, 2012. DOI: 10.1002/smll.201102635.

[51] Vanesa C. Sanchez, Ashish Jachak, Robert H. Hurt, and Agnes B. Kane. Biological interactions of graphene-family nanomaterials: an interdisciplinary review. *Chemical Research in Toxicology*, 25(1):15–34, 2012. DOI: 10.1021/tx200339h.

[52] Th. Seyller, K. V. Emtsev, K. Gao, F. Speck, L. Ley, A. Tadich, L. Broekman, J. D. Riley, R. C. G. Leckey, O. Rader, A. Varykhalov, and A. M. Shikin. Structural and electronic properties of graphite layers grown on sic(0001). *Surface Science*, 600(18, SI):3906–3911, 2006. DOI: 10.1016/j.susc.2006.01.102. 23rd European Conference on Surface Science (ECOSS-23), Freie Univ, Berlin, Germany, SEP 04-09, 2005.

[53] Taisuke Ohta, Aaron Bostwick, Thomas Seyller, Karsten Horn, and Eli Rotenberg. Controlling the electronic structure of bilayer graphene. *Science*, 313(5789):951–954, 2006. DOI: 10.1126/science.1130681.

[54] Th. Seyller, K. V. Emtsev, F. Speck, K. -Y. Gao, and L. Ley. Schottky barrier between 6h-sic and graphite: implications for metal/sic contact formation. *Applied Physics Letters*, 88(24):242103, 2006. DOI: 10.1063/1.2213928.

[55] D. A. Siegel, C. G. Hwang, A. V. Fedorov, and A. Lanzara. Quasifreestanding multilayer graphene films on the carbon face of sic. *Physical Review B*, 81(24), 2010. DOI: 10.1103/PhysRevB.81.241417.

[56] Xiaojun Weng, Joshua A. Robinson, Kathleen Trumbull, Randall Cavalero, Mark A. Fanton, and David Snyder. Epitaxial graphene on sic(000(1)over-bar): stacking order and interfacial structure. *Applied Physics Letters*, 100(3):031904, 2012. DOI: 10.1063/1.3678021.

[57] M. Orlita, C. Faugeras, J. M. Schneider, G. Martinez, D. K. Maude, and M. Potemski. Graphite from the viewpoint of landau level spectroscopy: an effective graphene bilayer and monolayer. *Physical Review Letters*, 102(16):166401, 2009. DOI: 10.1103/PhysRevLett.102.166401.

[58] Leif I. Johansson, Rickard Armiento, Jose Avila, Chao Xia, Stephan Lorcy, Igor A. Abrikosov, Maria C. Asensio, and Chariya Virojanadara. Multiple pi-bands and bernal stacking of multilayer graphene on c-face sic, revealed by nano-angle resolved photoemission. *Scientific Reports*, 4:4157, 2014. DOI: 10.1038/srep04157.

[59] M. Sprinkle, J. Hicks, A. Tejeda, A. Taleb-Ibrahimi, P. Le Fevre, F. Bertran, H. Tinkey, M. C. Clark, P. Soukiassian, D. Martinotti, J. Hass, and E. H. Conrad. Multilayer epitaxial graphene grown on the sic (000(1)over-bar) surface; structure and electronic properties. *Journal of Physics D-Applied Physics*, 43(37):374006, 2010. DOI: 10.1088/0022-3727/43/37/374006.

[60] A. Tejeda, A. Taleb-Ibrahimi, W. de Heer, C. Berger, and E. H. Conrad. Electronic structure of epitaxial graphene grown on the c-face of sic and its relation to the structure. *New Journal of Physics*, 14:125007, 2012. DOI: 10.1088/1367-2630/14/12/125007.

[61] Dong Sun, Charles Divin, Claire Berger, Walt A. de Heer, Phillip N. First, and Theodore B. Norris. Spectroscopic measurement of interlayer screening in multilayer epitaxial graphene. *Physical Review Letters*, 104(13):136802, 2010. DOI: 10.1103/PhysRevLett.104.136802.

[62] W. Norimatsu and M. Kusunoki. Formation process of graphene on sic (0001). *Physica E-Low-Dimensional Systems & Nanostructures*, 42(4):691–694, 2010. DOI: 10.1016/j.physe.2009.11.151. 18th International Conference on Electronic Properties of Two-Dimensional Systems, Kobe, Japan, JUL 19-24, 2009.

[63] Wataru Norimatsu, Juji Takada, and Michiko Kusunoki. Formation mechanism of graphene layers on sic (000(1)over-bar) in a high-pressure argon atmosphere. *Physical Review B*, 84(3):035424, 2011. DOI: 10.1103/PhysRevB.84.035424.

[64] J. S. Moon, D. Curtis, M. Hu, D. Wong, C. McGuire, P. M. Campbell, G. Jernigan, J. L. Tedesco, B. VanMil, R. Myers-Ward, C. Eddy Jr., and D. K. Gaskill. Epitaxial-graphene rf field-effect transistors on si-face 6h-sic substrates. *IEEE Electron Device Letters*, 30(6):650–652, 2009. DOI: 10.1109/LED.2009.2020699.

[65] N. Y. Garces, V. D. Wheeler, J. K. Hite, G. G. Jernigan, J. L. Tedesco, Neeraj Nepal, C. R. Eddy Jr., and D. K. Gaskill. Epitaxial graphene surface preparation for atomic layer deposition of al2o3. *Journal of Applied Physics*, 109(12):124304, 2011. DOI: 10.1063/1.3596761.

[66] J. S. Moon, H-C. Seo, M. Antcliffe, D. Le, C. McGuire, A. Schmitz, L. O. Nyakiti, D. K. Gaskill, P. M. Campbell, K-M. Lee, and P. Asbeck. Graphene fets for zero-bias linear resistive fet mixers. *IEEE Electron Device Letters*, 34(3):465–467, 2013. DOI: 10.1109/LED.2012.2236533.

[67] Nelson Y. Garces, Virginia D. Wheeler, and D. Kurt Gaskill. Graphene functionalization and seeding for dielectric deposition and device integration. *Journal of Vacuum Science & Technology B*, 30(3):030801, 2012. DOI: 10.1116/1.3693416.

[68] Aaron Bostwick, Taisuke Ohta, Thomas Seyller, Karsten Horn, and Eli Rotenberg. Quasiparticle dynamics in graphene. *Nature Physics*, 3(1):36–40, 2007. DOI: 10.1038/nphys477.

[69] S. Y. Zhou, G.-H. Gweon, A. V. Fedorov, P. N. First, W. A. De Heer, D.-H. Lee, F. Guinea, A. H. Castro Neto, and A. Lanzara. Substrate-induced bandgap opening in epitaxial graphene. *Nature Materials*, 6(10):770–775, 2007. DOI: 10.1038/nmat2003.

[70] S. Y. Zhou, G.-H. Gweon, A. V. Fedorov, P. N. First, W. A. De Heer, D.-H. Lee, F. Guinea, A. H. Castro Neto, and A. Lanzara. Substrate-induced bandgap opening in epitaxial graphene. *Nature Materials*, 6(11):916, 2007. DOI: 10.1038/nmat2056.

[71] S. Y. Zhou, D. A. Siegel, A. V. Fedorov, F. El Gabaly, A. K. Schmid, A. H. Castro Neto, D. -H. Lee, and A. Lanzara. Origin of the energy bandgap in epitaxial graphene - reply. *Nature Materials*, 7(4):259–260, 2008. DOI: 10.1038/nmat2154b.

[72] Aaron Bostwick, Taisuke Ohta, Jessica L. McChesney, Thomas Seyller, Karsten Horn, and Eli Rotenberg. Renormalization of graphene bands by many-body interactions. *Solid State Communications*, 143(1-2):63–71, 2007. DOI: 10.1016/j.ssc.2007.04.034.

[73] Aaron Bostwick, Taisuke Ohta, Jessica L. McChesney, Konstantin V. Emtsev, Florian Speck, Thomas Seyller, Karsten Horn, Stephan D. Kevan, and Eli Rotenberg. The interaction of quasi-particles in graphene with chemical dopants. *New Journal of Physics*, 12:125014, 2010. DOI: 10.1088/1367-2630/12/12/125014.

[74] Aaron Bostwick, Florian Speck, Thomas Seyller, Karsten Horn, Marco Polini, Reza Asgari, Allan H. MacDonald, and Eli Rotenberg. Observation of plasmarons in quasi-freestanding doped graphene. *Science*, 328(5981):999–1002, 2010. DOI: 10.1126/science.1186489.

[75] Andrew L. Walter, Aaron Bostwick, Ki-Joon Jeon, Florian Speck, Markus Ostler, Thomas Seyller, Luca Moreschini, Young Jun Chang, Marco Polini, Reza Asgari, Allan H. MacDonald, Karsten Horn, and Eli Rotenberg. Effective screening and the plasmaron bands in graphene. *Physical Review B*, 84(8):085410, 2011. DOI: 10.1103/PhysRevB.84.085410.

[76] Konstantin V. Emtsev, Aaron Bostwick, Karsten Horn, Johannes Jobst, Gary L. Kellogg, Lothar Ley, Jessica L. McChesney, Taisuke Ohta, Sergey A. Reshanov, Jonas Roehrl, Eli Rotenberg, Andreas K. Schmid, Daniel Waldmann, Heiko B. Weber, and Thomas Seyller. Towards wafer-size graphene layers by atmospheric pressure graphitization of silicon carbide. *Nature Materials*, 8(3):203–207, 2009. DOI: 10.1038/NMAT2382.

[77] Walt A. de Heer, Claire Berger, Ming Ruan, Mike Sprinkle, Xuebin Li, Yike Hu, Baiqian Zhang, John Hankinson, and Edward Conrad. Large area and structured epitaxial graphene produced by confinement controlled sublimation of silicon carbide. *Proceedings of the National Academy of Sciences of the United States of America*, 108(41):16900–16905, 2011. DOI: 10.1073/pnas.1105113108.

[78] J. Roehrl, M. Hundhausen, K. V. Emtsev, Th. Seyller, R. Graupner, and L. Ley. Raman spectra of epitaxial graphene on sic(0001). *Applied Physics Letters*, 92(20):201918, 2008. DOI: 10.1063/1.2929746.

[79] T. Filleter, K. V. Emtsev, Th. Seyller, and R. Bennewitz. Local work function measurements of epitaxial graphene. *Applied Physics Letters*, 93(13):133117, 2008. DOI: 10.1063/1.2993341.

[80] H. Hibino, H. Kageshima, F. Maeda, M. Nagase, Y. Kobayashi, and H. Yamaguchi. Microscopic thickness determination of thin graphite films formed on sic from quantized oscillation in reflectivity of low-energy electrons. *Physical Review B*, 77(7):075413, 2008. DOI: 10.1103/PhysRevB.77.075413.

[81] C. Riedl, C. Coletti, T. Iwasaki, A. A. Zakharov, and U. Starke. Quasi-free-standing epitaxial graphene on sic obtained by hydrogen intercalation. *Physical Review Letters*, 103(24):246804, 2009. DOI: 10.1103/PhysRevLett.103.246804.

[82] Florian Speck, Markus Ostler, Sven Besendoerfer, Julia Krone, Martina Wanke, and Thomas Seyller. Growth and intercalation of graphene on silicon carbide studied by low-energy electron microscopy. *Annalen der Physik*, 529(11, SI):1700046, 2017. DOI: 10.1002/andp.201700046.

[83] Myriano H. Oliveira Jr., Timo Schumann, Felix Fromm, Roland Koch, Markus Ostler, Manfred Ramsteiner, Thomas Seyller, Joao Marcelo J. Lopes, and Henning Riechert. Formation of high-quality quasi-free-standing bilayer graphene on sic(0001) by oxygen intercalation upon annealing in air. *Carbon*, 52:83–89, 2013. DOI: 10.1016/j.carbon.2012.09.008.

[84] Markus Ostler, Felix Fromm, Roland J. Koch, Peter Wehrfritz, Florian Speck, Hendrik Vita, Stefan Boettcher, Karsten Horn, and Thomas Seyller. Buffer layer free graphene on sic(0001) via interface oxidation in water vapor. *Carbon*, 70:258–265, 2014. DOI: 10.1016/j.carbon.2014.01.004.

[85] Tatsuya Sumi, Kazuki Nagai, Jianfeng Bao, Tomo-o Terasawa, Wataru Norimatsu, Michiko Kusunoki, and Yusuke Wakabayashi. Structure of quasi-free-standing graphene on the sic (0001) surface prepared by the rapid cooling method. *Applied Physics Letters*, 117(14):143102, 2020. DOI: 10.1063/5.0021071.

[86] F. Speck, J. Jobst, F. Fromm, M. Ostler, D. Waldmann, M. Hundhausen, H. B. Weber, and Th. Seyller. The quasi-free-standing nature of graphene on h-saturated sic(0001). *Applied Physics Letters*, 99(12):122106, 2011. DOI: 10.1063/1.3643034.

[87] Yu Liu, R. F. Willis, K. V. Emtsev, and Th. Seyller. Plasmon dispersion and damping in electrically isolated two-dimensional charge sheets. *Physical Review B*, 78(20):201403, 2008. DOI: 10.1103/PhysRevB.78.201403.

[88] R. J. Koch, Th. Seyller, and J. A. Schaefer. Strong phonon-plasmon coupled modes in the graphene/silicon carbide heterosystem. *Physical Review B*, 82(20):201413, 2010. DOI: 10.1103/PhysRevB.82.201413.

[89] Johannes Jobst, Daniel Waldmann, Florian Speck, Roland Hirner, Duncan K. Maude, Thomas Seyller, and Heiko B. Weber. Transport properties of high-quality epitaxial graphene on 6h-sic(0001). *Solid State Communications*, 151(16, SI):1061–1064, 2011. DOI: 10.1016/j.ssc.2011.05.015.

[90] I. Crassee, M. Orlita, M. Potemski, A. L. Walter, M. Ostler, Th. Seyller, I. Gaponenko, J. Chen, and A. B. Kuzmenko. Intrinsic terahertz plasmons and magnetoplasmons in large scale monolayer graphene. *Nano Letters*, 12(5):2470–2474, 2012. DOI: 10.1021/nl300572y.

[91] Jianing Chen, Maxim L. Nesterov, Alexey Yu Nikitin, Sukosin Thongrattanasiri, Pablo Alonso-Gonzalez, Tetiana M. Slipchenko, Florian Speck, Markus Ostler, Thomas Seyller, Iris Crassee, Frank H. L. Koppens, Luis Martin-Moreno, F. Javier Garcia de Abajo, Alexey B. Kuzmenko, and Rainer Hillenbrand. Strong plasmon reflection at nanometer-size gaps in monolayer graphene on sic. *Nano Letters*, 13(12):6210–6215, 2013. DOI: 10.1021/nl403622t.

[92] Xinghan Cai, Andrei B. Sushkov, Mohammad M. Jadidi, Luke Nyakiti, Rachael L. Myers-Ward, D. Kurt Gaskill, Thomas E. Murphy, Michael S. Fuhrer, and H. Dennis Drew. Plasmon-enhanced terahertz photodetection in graphene. *Nano Letters*, 15(7):4295–4302, 2015. DOI: 10.1021/acs.nanolett.5b00137.

[93] Johannes Jobst, Daniel Waldmann, Florian Speck, Roland Hirner, Duncan K. Maude, Thomas Seyller, and Heiko B. Weber. Quantum oscillations and quantum hall effect in epitaxial graphene. *Physical Review B*, 81(19):195434, 2010. DOI: 10.1103/PhysRevB.81.195434.

[94] A. J. M. Giesbers, P. Prochazka, and C. F. J. Flipse. Surface phonon scattering in epitaxial graphene on 6h-sic. *Physical Review B*, 87(19):195405, 2013. DOI: 10.1103/PhysRevB.87.195405.

[95] Juergen Ristein, Wenying Zhang, Florian Speck, Markus Ostler, Lothar Ley, and Thomas Seyller. Characteristics of solution gated field effect transistors on the basis of epitaxial graphene on silicon carbide. *Journal of Physics D-Applied Physics*, 43(34):345303, 2010. DOI: 10.1088/0022-3727/43/34/345303.

[96] Jingjing Lin, Liwei Guo, Yuping Jia, Rong Yang, Shuang Wu, Jiao Huang, Yu Guo, Zhilin Li, Guangyu Zhang, and Xiaolong Chen. Identification of dominant scattering mechanism in epitaxial graphene on sic. *Applied Physics Letters*, 104(18):183102, 2014. DOI: 10.1063/1.4875384.

[97] F. Krach, S. Hertel, D. Waldmann, J. Jobst, M. Krieger, S. Reshanov, A. Schoner, and H. B. Weber. A switch for epitaxial graphene electronics: utilizing the silicon carbide substrate as transistor channel. *Applied Physics Letters*, 100(12):122102, 2012. DOI: 10.1063/1.3695157.

[98] S. Hertel, D. Waldmann, J. Jobst, A. Albert, M. Albrecht, S. Reshanov, A. Schoner, M. Krieger, and H. B. Weber. Tailoring the graphene/silicon carbide interface for monolithic wafer-scale electronics. *Nature Communications*, 3:957, 2012. DOI: 10.1038/ncomms1955.

[99] Daniel Waldmann, Johannes Jobst, Florian Speck, Thomas Seyller, Michael Krieger, and Heiko B. Weber. Bottom-gated epitaxial graphene. *Nature Materials*, 10(5):357–360, 2011. DOI: 10.1038/NMAT2988.

[100] A. J. M. Giesbers, K. Uhlirova, M. Konecny, E. C. Peters, M. Burghard, J. Aarts, and C. F. J. Flipse. Interface-induced room-temperature ferromagnetism in hydrogenated epitaxial graphene. *Physical Review Letters*, 111(16):166101, 2013. DOI: 10.1103/PhysRevLett.111.166101.

[101] Mohamed Ridene, Ameneh Najafi, and Kees Flipse. Origin of room-temperature ferromagnetism in hydrogenated epitaxial graphene on silicon carbide. *Nanomaterials*, 9(2):228, 2019. DOI: 10.3390/nano9020228.

[102] Iris Crassee, Julien Levallois, Andrew L. Walter, Markus Ostler, Aaron Bostwick, Eli Rotenberg, Thomas Seyller, Dirk van der Marel, and Alexey B. Kuzmenko. Giant faraday rotation in single- and multilayer graphene. *Nature Physics*, 7(1):48–51, 2011. DOI: 10.1038/NPHYS1816.

[103] I. Crassee, J. Levallois, D. van der Marel, A. L. Walter, Th. Seyller, and A. B. Kuzmenko. Multicomponent magneto-optical conductivity of multilayer graphene on sic. *Physical Review B*, 84(3):035103, 2011. DOI: 10.1103/PhysRevB.84.035103.

[104] M. Orlita, I. Crassee, C. Faugeras, A. B. Kuzmenko, F. Fromm, M. Ostler, Th Seyller, G. Martinez, M. Polini, and M. Potemski. Classical to quantum crossover of the cyclotron resonance in graphene: a study of the strength of intraband absorption. *New Journal of Physics*, 14:095008, 2012. DOI: 10.1088/1367-2630/14/9/095008.

[105] Thomas Maassen, J. Jasper van den Berg, Natasja IJbema, Felix Fromm, Thomas Seyller, Rositza Yakimova, and Bart J. van Wees. Long spin relaxation times in wafer scale epitaxial graphene on sic(0001). *Nano Letters*, 12(3):1498–1502, 2012. DOI: 10.1021/nl2042497.

[106] Alexander Tzalenchuk, Samuel Lara-Avila, Alexei Kalaboukhov, Sara Paolillo, Mikael Syvajarvi, Rositza Yakimova, Olga Kazakova, T. J. B. M. Janssen, Vladimir Fal'ko, and Sergey Kubatkin. Towards a quantum resistance standard based on epitaxial graphene. *Nature Nanotechnology*, 5(3):186–189, 2010. DOI: 10.1038/NNANO.2009.474.

[107] Sofia Aslanidou, Alberto Garcia-Garcia, Philippe Godignon, and Gemma Rius. Electronic interface and charge carrier density in epitaxial graphene on silicon carbide. a review on metal-graphene contacts and electrical gating. *APL Materials*, 8(10):100702, 2020. DOI: 10.1063/5.0022341.

[108] Aiswarya Pradeepkumar, D. Kurt Gaskill, and Francesca Iacopi. Electronic and transport properties of epitaxial graphene on sic and 3c-sic/si: a review. *Applied Sciences-Basel*, 10(12):4350, 2020. DOI: 10.3390/app10124350.

[109] Mattias Kruskopf, Davood Momeni Pakdehi, Klaus Pierz, Stefan Wundrack, Rainer Stosch, Thorsten Dziomba, Martin Goetz, Jens Baringhaus, Johannes Aprojanz, Christoph Tegenkamp, Jakob Lidzba, Thomas Seyller, Frank Hohls, Franz J. Ahlers, and Hans W. Schumacher. Comeback of epitaxial graphene for electronics: large-area growth of bilayer-free graphene on sic. *2D Materials*, 3(4):041002, 2016. DOI: 10.1088/2053-1583/3/4/041002.

[110] Hans He, Kyung Ho Kim, Andrey Danilov, Domenico Montemurro, Liyang Yu, Yung Woo Park, Floriana Lombardi, Thilo Bauch, Kasper Moth-Poulsen, Tihomir Lakimov, Rositsa Yakimova, Per Malmberg, Christian Muller, Sergey Kubatkin, and Samuel Lara-Avila. Uniform doping of graphene close to the dirac point by polymer-assisted assembly of molecular dopants. *Nature Communications*, 9:3956, 2018. DOI: 10.1038/s41467-018-06352-5.

[111] Bingyan Chen, Huixin Huang, Xiaomeng Ma, Le Huang, Zhiyong Zhang, and Lian-Mao Peng. How good can cvd-grown monolayer graphene be? *Nanoscale*, 6(24):15255–15261, 2014. DOI: 10.1039/c4nr05664g.

[112] Cheol-Hwan Park and Nicola Marzari. Berry phase and pseudospin winding number in bilayer graphene. *Physical Review B*, 84(20):205440, 2011. DOI: 10.1103/PhysRevB.84.205440.

[113] Di Xiao, Ming-Che Chang, and Qian Niu. Berry phase effects on electronic properties. *Reviews of Modern Physics*, 82(3):1959–2007, 2010. DOI: 10.1103/RevModPhys.82.1959.

[114] K. S. Novoselov, Z. Jiang, Y. Zhang, S. V. Morozov, H. L. Stormer, U. Zeitler, J. C. Maan, G. S. Boebinger, P. Kim, and A. K. Geim. Room-temperature quantum hall effect in graphene. *Science*, 315(5817):1379, 2007. DOI: 10.1126/science.1137201.

[115] R. R. Nair, P. Blake, A. N. Grigorenko, K. S. Novoselov, T. J. Booth, T. Stauber, N. M. R. Peres, and A. K. Geim. Fine structure constant defines visual transparency of graphene. *Science*, 320(5881):1308, 2008. DOI: 10.1126/science.1156965.

[116] Kirill I. Bolotin, Fereshte Ghahari, Michael D. Shulman, Horst L. Stormer, and Philip Kim. Observation of the fractional quantum hall effect in graphene. *Nature*, 462(7270):196–199, 2009. DOI: 10.1038/nature08582.

[117] Xu Du, Ivan Skachko, Fabian Duerr, Adina Luican, and Eva Y. Andrei. Fractional quantum hall effect and insulating phase of dirac electrons in graphene. *Nature*, 462(7270):192–195, 2009. DOI: 10.1038/nature08522.

[118] K. S. Novoselov, V. I. Fal'ko, L. Colombo, P. R. Gellert, M. G. Schwab, and K. Kim. A roadmap for graphene. *Nature*, 490(7419):192–200, 2012. DOI: 10.1038/nature11458.

[119] Jonathan K. Wassei and Richard B. Kaner. Graphene, a promising transparent conductor. *Materials Today*, 13(3):52–59, 2010. DOI: 10.1016/S1369-7021(10)70034-1.

[120] J. B. Khurgin. Graphene-a rather ordinary nonlinear optical material. *Applied Physics Letters*, 104(16):161116, 2014. DOI: 10.1063/1.4873704.

[121] S. A. Mikhailov. Comment on "graphene-a rather ordinary nonlinear optical material" [appl. phys. lett. 104, 161116 (2014)]. *Applied Physics Letters*, 111(10):106101, 2017. DOI: 10.1063/1.4997849.

[122] Jacob B. Khurgin. Response to "comment on 'graphene-a rather ordinary nonlinear optical material'" [appl. phys. lett. 111, 106101 (2017)]. *Applied Physics Letters*, 111(10):106102, 2017. DOI: 10.1063/1.4999183.

[123] T. J. B. M. Janssen, S. Rozhko, I. Antonov, A. Tzalenchuk, J. M. Williams, Z. Melhem, H. He, S. Lara-Avila, S. Kubatkin, and R. Yakimova. Operation of graphene quantum hall resistance standard in a cryogen-free table-top system. *2D Materials*, 2(3):035015, 2015. DOI: 10.1088/2053-1583/2/3/035015.

[124] Andrea C. Ferrari, Francesco Bonaccorso, Vladimir Fal'ko, Konstantin S. Novoselov, Stephan Roche, Peter Boggild, Stefano Borini, Frank H. L. Koppens, Vincenzo Palermo, Nicola Pugno, Jose A. Garrido, Roman Sordan, Alberto Bianco, Laura Ballerini, Maurizio Prato, Elefterios Lidorikis, Jani Kivioja, Claudio Marinelli, Tapani Ryhaenen, Alberto Morpurgo, Jonathan N. Coleman, Valeria Nicolosi, Luigi Colombo, Albert Fert, Mar Garcia-Hernandez, Adrian Bachtold, Gregory F. Schneider, Francisco Guinea, Cees Dekker, Matteo Barbone, Zhipei Sun, Costas Galiotis, Alexander N. Grigorenko, Gerasimos Konstantatos, Andras Kis, Mikhail Katsnelson, Lieven Vandersypen, Annick Loiseau, Vittorio Morandi, Daniel Neumaier, Emanuele Treossi, Vittorio Pellegrini, Marco Polini, Alessandro Tredicucci, Gareth M. Williams, Byung Hee Hong, Jong-Hyun

Ahn, Jong Min Kim, Herbert Zirath, Bart J. van Wees, Herre van der Zant, Luigi Occhipinti, Andrea Di Matteo, Ian A. Kinloch, Thomas Seyller, Etienne Quesnel, Xinliang Feng, Ken Teo, Nalin Rupesinghe, Pertti Hakonen, Simon R. T. Neil, Quentin Tannock, Tomas Loefwander, and Jari Kinaret. Science and technology roadmap for graphene, related two-dimensional crystals, and hybrid systems. *Nanoscale*, 7(11):4598–4810, 2015. DOI: 10.1039/c4nr01600a.

[125] Alessandro De Cecco, Vladimir S. Prudkovskiy, David Wander, Rini Ganguly, Claire Berger, Walt A. de Heer, Herve Courtois, and Clemens B. Winkelmann. Non-invasive nanoscale potentiometry and ballistic transport in epigraphene nanoribbons. *Nano Letters*, 20(5):3786–3790, 2020. DOI: 10.1021/acs.nanolett.0c00838.

[126] Hans He, Samuel Lara-Avila, Kyung Ho Kim, Nick Fletcher, Sergiy Rozhko, Tobias Bergsten, Gunnar Eklund, Karin Cedergren, Rositsa Yakimova, Yung Woo Park, Alexander Tzalenchuk, and Sergey Kubatkin. Polymer-encapsulated molecular doped epigraphene for quantum resistance metrology. *Metrologia*, 56(4):045004, 2019. DOI: 10.1088/1681-7575/ab2807.

[127] L. Wang, I. Meric, P. Y. Huang, Q. Gao, Y. Gao, H. Tran, T. Taniguchi, K. Watanabe, L. M. Campos, D. A. Muller, J. Guo, P. Kim, J. Hone, K. L. Shepard, and C. R. Dean. One-dimensional electrical contact to a two-dimensional material. *Science*, 342(6158):614–617, 2013. DOI: 10.1126/science.1244358.

[128] P. Neugebauer, M. Orlita, C. Faugeras, A. -L. Barra, and M. Potemski. How perfect can graphene be? *Physical Review Letters*, 103(13):136403, 2009. DOI: 10.1103/PhysRevLett.103.136403.

[129] Luca Banszerus, Michael Schmitz, Stephan Engels, Jan Dauber, Martin Oellers, Federica Haupt, Kenji Watanabe, Takashi Taniguchi, Bernd Beschoten, and Christoph Stampfer. Ultrahigh-mobility graphene devices from chemical vapor deposition on reusable copper. *Science Advances*, 1(6):e1500222, 2015. DOI: 10.1126/sciadv.1500222.

[130] Domenico De Fazio, David G. Purdie, Anna K. Ott, Philipp Braeuninger-Weimer, Timofiy Khodkov, Stijn Goossens, Takashi Taniguchi, Kenji Watanabe, Patrizia Livreri, Frank H. L. Koppens, Stephan Hofmann, Ilya Goykhman, Andrea C. Ferrari, and Antonio Lombardo. High-mobility, wet-transferred graphene grown by chemical vapor deposition. *ACS Nano*, 13(8):8926–8935, 2019. DOI: 10.1021/acsnano.9b02621.

[131] H. Fukidome, Y. Kawai, F. Fromm, M. Kotsugi, H. Handa, T. Ide, T. Ohkouchi, H. Miyashita, Y. Enta, T. Kinoshita, Th Seyller, and M. Suemitsu. Precise control of epitaxy of graphene by microfabricating sic substrate. *Applied Physics Letters*, 101(4):041605, 2012. DOI: 10.1063/1.4740271.

[132] Maria T. Schlecht, Sascha Preu, Stefan Malzer, and Heiko B. Weber. An efficient terahertz rectifier on the graphene/sic materials platform. *Scientific Reports*, 9:11205, 2019. DOI: 10.1038/s41598-019-47606-6.

[133] M. Conrad, J. Rault, Y. Utsumi, Y. Garreau, A. Vlad, A. Coati, J. -P. Rueff, P. F. Miceli, and E. H. Conrad. Structure and evolution of semiconducting buffer graphene grown on sic(0001). *Physical Review B*, 96(19):195304, 2017. DOI: 10.1103/PhysRevB.96.195304.

[134] Jonathan D. Emery, Virginia H. Wheeler, James E. Johns, Martin E. McBriarty, Blanka Detlefs, Mark C. Hersam, D. Kurt Gaskill, and Michael J. Bedzyk. Structural consequences of hydrogen intercalation of epitaxial graphene on sic(0001). *Applied Physics Letters*, 105(16):161602, 2014. DOI: 10.1063/1.4899142.

[135] Shinichi Tanabe, Makoto Takamura, Yuichi Harada, Hiroyuki Kageshima, and Hiroki Hibino. Effects of hydrogen intercalation on transport properties of quasi-free-standing monolayer graphene. *Japanese Journal of Applied Physics*, 53(4, SI):04EN01, 2014. DOI: 10.7567/JJAP.53.04EN01.

[136] Yanfei Yang, Lung-I. Huang, Yasuhiro Fukuyama, Fan-Hung Liu, Mariano A. Real, Paola Barbara, Chi-Te Liang, David B. Newell, and Randolph E. Elmquist. Low carrier density epitaxial graphene devices on sic. *Small*, 11(1):90–95, 2015. DOI: 10.1002/smll.201400989.

[137] J. Ristein, S. Mammadov, and Th Seyller. Origin of doping in quasi-free-standing graphene on silicon carbide. *Physical Review Letters*, 108(24):246104, 2012. DOI: 10.1103/PhysRevLett.108.246104.

[138] Zhen-Yu Juang, Chih-Yu Wu, Chien-Wei Lo, Wei-Yu Chen, Chih-Fang Huang, Jenn-Chang Hwang, Fu-Rong Chen, Keh-Chyang Leou, and Chuen-Horng Tsai. Synthesis of graphene on silicon carbide substrates at low temperature. *Carbon*, 47(8):2026–2031, 2009. DOI: 10.1016/j.carbon.2009.03.051.

[139] Muhammed Emre Ayhan, Golap Kalita, Remi Papon, Ryo Hirano, and Masaki Tanemura. Synthesis of transfer-free graphene by solid phase reaction process in presence of a carbon diffusion barrier. *Materials Letters*, 129:76–79, 2014. DOI: 10.1016/j.matlet.2014.05.007.

[140] Gedeng Ruan, Zhengzong Sun, Zhiwei Peng, and James M. Tour. Growth of graphene from food, insects, and waste. *ACS Nano*, 5(9):7601–7607, 2011. DOI: 10.1021/nn202625c.

[141] Wang Can, Zhan Liang, Qiao Wen-ming, and Ling Li-cheng. Preparation of graphene nanosheets through detonation. *New Carbon Materials*, 26(1):21–25, 2011. DOI: 10.1016/S1872-5805(11)60063-2.

[142] Gholam Reza Yazdi, Tihomir Iakimov, and Rositsa Yakimova. Epitaxial graphene on sic: a review of growth and characterization. *Crystals*, 6(5):53, 2016. DOI: 10.3390/cryst6050053.

[143] B. K. Daas, Sabih U. Omar, S. Shetu, Kevin M. Daniels, S. Ma, T. S. Sudarshan, and M. V. S. Chandrashekhar. Comparison of epitaxial graphene growth on polar and nonpolar 6h-sic faces: on the growth of multilayer films. *Crystal Growth & Design*, 12(7):3379–3387, 2012. DOI: 10.1021/cg300456v.

[144] J. Hass, F. Varchon, J. E. Millan-Otoya, M. Sprinkle, N. Sharma, W. A. De Heer, C. Berger, P. N. First, L. Magaud, and E. H. Conrad. Why multilayer graphene on 4h-sic(000(1)over-bar) behaves like a single sheet of graphene. *Physical Review Letters*, 100(12):125504, 2008. DOI: 10.1103/PhysRevLett.100.125504.

[145] M. Sprinkle, D. Siegel, Y. Hu, J. Hicks, A. Tejeda, A. Taleb-Ibrahimi, P. Le Fevre, F. Bertran, S. Vizzini, H. Enriquez, S. Chiang, P. Soukiassian, C. Berger, W. A. de Heer, A. Lanzara, and E. H. Conrad. First direct observation of a nearly ideal graphene band structure. *Physical Review Letters*, 103(22):226803, 2009. DOI: 10.1103/PhysRevLett.103.226803.

[146] M. Sprinkle, M. Ruan, Y. Hu, J. Hankinson, M. Rubio-Roy, B. Zhang, X. Wu, C. Berger, and W. A. de Heer. Scalable templated growth of graphene nanoribbons on sic. *Nature Nanotechnology*, 5(10):727–731, 2010. DOI: 10.1038/nnano.2010.192.

[147] K. V. Emtsev, F. Speck, Th. Seyller, L. Ley, and J. D. Riley. Interaction, growth, and ordering of epitaxial graphene on sic{0001} surfaces: a comparative photoelectron spectroscopy study. *Physical Review B*, 77(15):155303, 2008. DOI: 10.1103/PhysRevB.77.155303.

[148] C. Riedl, U. Starke, J. Bernhardt, M. Franke, and K. Heinz. Structural properties of the graphene-sic(0001) interface as a key for the preparation of homogeneous large-terrace graphene surfaces. *Physical Review B*, 76(24):245406, 2007. DOI: 10.1103/PhysRevB.76.245406.

[149] Samir Mammadov, Juergen Ristein, Julia Krone, Christian Raidel, Martina Wanke, Veit Wiesmann, Florian Speck, and Thomas Seyller. Work function of graphene multilayers on sic(0001). *2D Materials*, 4(1):015043, 2017. DOI: 10.1088/2053-1583/4/1/015043.

[150] Wan Sik Hwang, Kristof Tahy, Luke O. Nyakiti, Virginia D. Wheeler, Rachael. L. Myers-Ward, C. R. Eddy Jr., D. Kurt Gaskill, Huili (Grace) Xing, Alan Seabaugh, and Debdeep Jena. Fabrication of top-gated epitaxial graphene nanoribbon fets using hydrogen-silsesquioxane. *Journal of Vacuum Science & Technology B*, 30(3):03D104, 2012. DOI: 10.1116/1.3693593.

[151] Johannes Aprojanz, Stephen R. Power, Pantelis Bampoulis, Stephan Roche, Antti-Pekka Jauho, Harold J. W. Zandvliet, Alexei A. Zakharov, and Christoph Tegenkamp. Ballistic tracks in graphene nanoribbons. *Nature Communications*, 9:4426, 2018. DOI: 10.1038/s41467-018-06940-5.

[152] Jens Baringhaus, Ming Ruan, Frederik Edler, Antonio Tejeda, Muriel Sicot, Amina Taleb-Ibrahimi, An-Ping Li, Zhigang Jiang, Edward H. Conrad, Claire Berger, Christoph Tegenkamp, and Walt A. de Heer. Exceptional ballistic transport in epitaxial graphene nanoribbons. *Nature*, 506(7488):349–354, 2014. DOI: 10.1038/nature12952.

[153] Mohammad M. Jadidi, Andrei B. Sushkov, Rachael L. Myers-Ward, Anthony K. Boyd, Kevin M. Daniels, D. Kurt Gaskill, Michael S. Fuhrer, H. Dennis Drew, and Thomas E. Murphy. Tunable terahertz hybrid metal-graphene plasmons. *Nano Letters*, 15(10):7099–7104, 2015. DOI: 10.1021/acs.nanolett.5b03191.

[154] Konrad Ullmann, Pedro B. Coto, Susanne Leitherer, Agustin Molina-Ontoria, Nazario Martin, Michael Thoss, and Heiko B. Weber. Single-molecule junctions with epitaxial graphene nanoelectrodes. *Nano Letters*, 15(5):3512–3518, 2015. DOI: 10.1021/acs.nanolett.5b00877.

[155] Abdel El Fatimy, Anindya Nath, Byoung Don Kong, Anthony K. Boyd, Rachael L. Myers-Ward, Kevin M. Daniels, M. Mehdi Jadidi, Thomas E. Murphy, D. Kurt Gaskill, and Paola Barbara. Ultra-broadband photodetectors based on epitaxial graphene quantum dots. *Nanophotonics*, 7(4):735–740, 2018. DOI: 10.1515/nanoph-2017-0100.

[156] Abdel El Fatimy, Rachael L. Myers-Ward, Anthony K. Boyd, Kevin M. Daniels, D. Kurt Gaskill, and Paola Barbara. Epitaxial graphene quantum dots for high-performance terahertz bolometers. *Nature Nanotechnology*, 11(4):335+, 2016. DOI: 10.1038/NNANO.2015.303.

[157] Kevin M. Daniels, M. Mehdi Jadidi, Andrei B. Sushkov, Anindya Nath, Anthony K. Boyd, Karthik Sridhara, H. Dennis Drew, Thomas E. Murphy, Rachael L. Myers-Ward, and D. Kurt Gaskill. Narrow plasmon resonances enabled by quasi-freestanding bilayer epitaxial graphene. *2D Materials*, 4(2):025034, 2017. DOI: 10.1088/2053-1583/aa5c75.

[158] D. Marchenko, A. Varykhalov, J. Sanchez-Barriga, Th. Seyller, and O. Rader. Rashba splitting of 100mev in au-intercalated graphene on sic. *Applied Physics Letters*, 108(17):172405, 2016. DOI: 10.1063/1.4947286.

[159] Takuya Higuchi, Christian Heide, Konrad Ullmann, Heiko B. Weber, and Peter Hommelhoff. Light-field-driven currents in graphene. *Nature*, 550(7675):224+, 2017. DOI: 10.1038/nature23900.

[160] Ferdinand Kisslinger, Christian Ott, Christian Heide, Erik Kampert, Benjamin Butz, Erdmann Spiecker, Sam Shallcross, and Heiko B. Weber. Linear magnetoresistance in mosaic-like bilayer graphene. *Nature Physics*, 11(8):650+, 2015. DOI: 10.1038/NPHYS3368.

[161] Johannes Jobst, Daniel Waldmann, Igor V. Gornyi, Alexander D. Mirlin, and Heiko B. Weber. Electron-electron interaction in the magnetoresistance of graphene. *Physical Review Letters*, 108(10):106601, 2012. DOI: 10.1103/PhysRevLett.108.106601.

[162] P. Lauffer, K. V. Emtsev, R. Graupner, Th. Seyller, L. Ley, S. A. Reshanov, and H. B. Weber. Atomic and electronic structure of few-layer graphene on sic(0001) studied with scanning tunneling microscopy and spectroscopy. *Physical Review B*, 77(15):155426, 2008. DOI: 10.1103/PhysRevB.77.155426.

[163] Wei Han, Roland K. Kawakami, Martin Gmitra, and Jaroslav Fabian. Graphene spintronics. *Nature Nanotechnology*, 9(10):794–807, 2014. DOI: 10.1038/NNANO.2014.214.

List of Abbreviations

- MBE...Molecular Beam Epitaxy
- GaAs...Gallium Arsenide
- CdTe...Cadmium Telluride
- SiC...Silicon Carbide
- CNT...Carbon Nanotube
- SiO_2...silicon dioxide
- BN...boron nitride
- IUPAC...International Union of Pure and Applied Chemistry
- ARPES...Angular Resolved Photo-Electron Spectroscopy
- HOPG...Highly Oriented/Ordered Pyrolytic Graphite
- AFM...Atomic Force Microscopy
- STM...Scanning Tunneling Microscopy
- LEED...Low-Energy Electron Diffraction
- CVD...Chemical Vapor Deposition
- MEG...Multi-Layer Epitaxial Graphene
- TEM...Transmission Electron Microscopy
- HREELS...High-Resolution Electron-Energy-Loss Spectroscopy
- F4-TCNQ...tetrafluorotetracyanoquinodimethane
- PMMA...polymethylmethacrylate
- NN...Nearest Neighbor
- NNN...Next Nearest Neighbor
- ITO...Indium Tin Oxide
- 2D...two-dimensional
- 1D...one-dimensional
- 0D...zero-dimensional
- THz...terahertz
- CMOS...Complementary Metal-Oxide-Semiconductor

- PASG...Polymer Assisted Sublimation Growth
- GNR...Graphene Nanoribbon
- SWGNR...Side-Wall Graphene Nanoribbon
- QFMLG...Quasi Free-standing Mono-Layer Graphene
- QFBLG...Quasi Free-standing Bilayer Graphene
- LO-phonon...longitudinal optical phonon
- ZO-phonon...out-of-plane optical phonon
- XUV...extreme ultraviolet
- TMD...transition metal dichalcogenide

List of Symbols

- B...magnetic field
- $\tilde{p}_x$, $\tilde{p}_y$, $\tilde{p}_z$...p-orbitals
- φ_1, φ_2, φ...basis wavefunctions
- b_1, b_2...linear coefficients
- $\mathbf{k}$...wavevector
- $u(\mathbf{r})$...function periodic with the crystal lattice, part of the Bloch wavefunction
- $\mathbf{r}$, $\mathbf{r_1}$, $\mathbf{r_2}$...position vector
- $\mathbf{a}_1$, $\mathbf{a}_2$...lattice basis vectors
- $\mathbf{R}$...lattice vector
- a_0...carbon-carbon nearest neighbor distance
- a...lattice constant
- n_1, n_2...integer multiples
- $\Psi_{\mathbf{k}}$...crystal wavefunction
- $\mathbf{p}$...momentum
- p_x, p_y, p_z...cartesian components of the momentum $\mathbf{p}$
- m_0...electron's mass in vacuum
- T...kinetic energy
- V, V_{at}...potential energy
- H...Hamiltonian
- E...Energy
- γ_1...intercation energy
- γ_0...overlap integral
- $\alpha(\mathbf{k}), \alpha(\mathbf{q}), \alpha(q, \vartheta)$...substitution function determining graphene's electronic band structure
- θ...phase of the complex function $\alpha(\mathbf{k})$
- ϵ_1...reference energy of carbon atoms
- ϑ...angle in polar coordinate system

- K, K'...high symmetry points in the 1^{st} Brillouin zone
- $\mathbf{K}$...wavevector of the K-point measured from the origin of the 1^{st} Brillouin zone
- $\mathbf{q}$, q...wavevector and its size measured from the K-point
- $\mathbf{e_{k_x}}$...unit vector in the $\mathbf{k_x}$ direction in the reciprocal space
- k_x...x-component of the wavevector $\mathbf{k}$
- $|n(\mathbf{r},t)\rangle$...stationary wavefunction
- $\Theta(t)$...phase of the wavefunction
- t...time
- σ_x, σ_y, σ_z...Pauli matrices
- v_F...Fermi velocity
- h...Planck constant
- $\hbar$...reduced Planck constant
- e...elementary charge
- ω_c...cyclotron resonance angular frequency
- ω...angular frequency
- i...complex unit
- $\mathbf{A}$...vector potential
- A_0...amplitude of the vector potential
- n, N...quantum numbers
- m^*...effective mass
- $W_{VB\rightarrow CB}$...transition rate from the valence band to the conduction band
- $\mathbf{E}$...electric field vector
- E_0...amplitude of the electric field
- τ...transition time
- W_a...absorbed power surface density
- W_i...power surface density of the incident radiation
- α...fine-structure constant
- T...optical transmission

- ε_0...permittivity of vacuum
- c...speed of light
- R_{xy}...Hall resistance
- ν...Landau level filling factor
- T_C...Curie temperature

A. Attachments

The attachments are the selected fifteen author's original papers [1, 2, 3, 4, 5, 6, 7, 8, 9, 10, 11, 12, 13, 14, 15].